INCORPORATION AND CHARACTERIZATION OF OPTICAL OXYGEN SENSORS IN SILICA AEROGEL MONOLITHS

By

Nathaniel Patrick Hawthorne

****

Submitted in partial fulfillment

of the requirements for

Honors in the Department of Chemistry

Union College

June, 2016

Abstract

HAWTHORNE, NATHANIEL P. Incorporation and characterization of optical oxygen sensors in silica aerogel monoliths, June 2016.

ADVISOR: Mary K. Carroll

This thesis presents the preparation and spectroscopic characterization of silica aerogel monoliths containing one or more types of entrapped luminescent species. We are characterizing the response of aerogel-platform sensors to environments with varying amounts of oxygen and investigating whether it is possible to detect changes in luminescence signal based on the movement of oxygen through the aerogel monoliths.

Our experiments indicate that for platinum(II) octaethylporphyrin (PtOEP) aerogels, the decrease in luminescence in the presence of oxygen is not linear with respect to the increase of concentration of oxygen. Various two-site models can be used to determine the accessibility of the PtOEP probes to oxygen. These techniques follow assumptions that the probes are located in two microenvironments, and either one or both of the microenvironments are accessible to oxygen. Data from both techniques indicate that the probes are accessible in only one microenvironment, with less than 10% inaccessible.

PtOEP-doped silica aerogels can be fabricated up to 3 ½ x 3 ½ x ½ “, and luminescence is optically visible when oxygen is removed. The path of the luminescence can be tracked through the sample, indicating that it might be possible to determine the flow rate of gases through aerogels by monitoring the rate of appearance of luminescence.

Contents

Table of Figures

Table of Tables

Introduction

I. Introduction at Aerogels

Oxygen gas is a molecule of great significance to human life and activities. Its impacts range from affecting the individual through human respiration and society through corrosion of infrastructure, to impacting the world with environmental processes. Being able to detect the presence of and change in concentration of such an important molecule would be significant. One such way to detect and monitor the change in oxygen concentration is through incorporating optical oxygen sensors (chemical probes) in various materials, including aerogels.

Aerogels are materials that are generally considered to be 90-99% air by volume, and have some of the lowest densities of any solids known. They were first theorized and then later manufactured by S.S. Kistler in 1931.[1] "Aerogel" is a generic name for a substance with such a high volume of air to volume; the backbone that comprises these solids can consist of a variety of elements. Silica aerogels in particular have many unique properties, including low thermal conductivity, sound conductivity as low as 100 m/s, and large specific surface areas that can exceed 1000 m^2/g.[2] Due to these and other properties, aerogels have a variety of uses from sound-proof floor insulation, to lunar dust collection, to serving as a medium for nuclear waste storage, and more.[3]

---

[1] SS Kistler. "Coherent expanded aerogels and jellies." *Nature* 127.3211 (1931): 741.

[2] B. Zhou, J. Shen, Y. Wu, G. Wu, and X. Ni. "Hydrophobic silica aerogels derived from polyethoxydisiloxane and perfluoroalkylsilane." *Materials Science and Engineering* 27.5-8 (2007): 1291-1294.

[3] A. C. Pierre and G. M. Pajonk. "Chemistry of Aerogels and Their Applications." *Chemical Reviews 102* (2002): 4243-4265.

II. Fabrication of aerogels

To prepare silica aerogels, one starts by preparing a wet gel mixture consisting of a silica matrix filled with solvent. Traditionally, two of the most commonly used silica precursors are tetramethyl orthosilicate (TMOS) and tetraethyl orthosilicate (TEOS). The structures for TMOS and TEOS are shown in Figure 1.

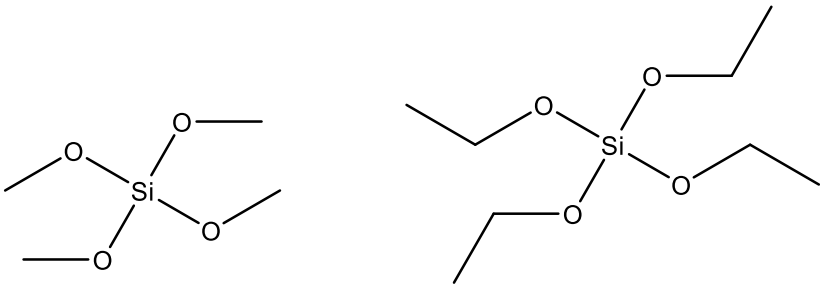

Figure 1: Line structures of TMOS (left) and TEOS (right), common precursors for silica aerogels.

The polymerization of silica alkoxides into silica aerogels comes about first through hydrolysis reactions and then condensation reactions to create a silicon oxide (silica) network. Aqueous acid or base is used as a catalyst in the hydrolysis of the silica species, and aqueous base is used to accelerate the condensation of the silica into a network.[4] This process is illustrated in Figure 2.

[4] A. C. Pierre and A. Rigacci. "SiO_2 Aerogels." *Aerogels Handbook.* Eds. M. A. Aegerter, N. Leventis, and M. M. Koebel.Springer Science+Business Media, 2011. 21-39.

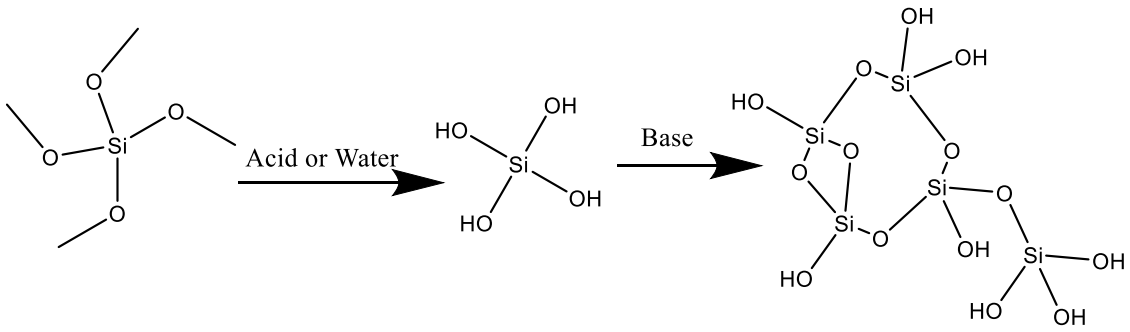

Figure 2: Schematic representation of hydrolysis and condensation of an alkoxide, TMOS.

After condensation, the solution forms a wet gel, with the solid silica backbone surrounded by the solvent mixture, which will be predominantly methanol, for TMOS-based gels, or ethanol, for TEOS-based gels. If the solvent evaporates out of the pores, the tension will cause the structure to suffer pore collapse, and the structure of the wet gel will shrink into a xerogel. If the wet gel can be dried so that the solvent can leave without causing pore collapse, the remaining structure is an aerogel, essentially identical in size and shape to the wet gel. A sketch of a wet-gel, xerogel and aerogel are shown in Figure 3.

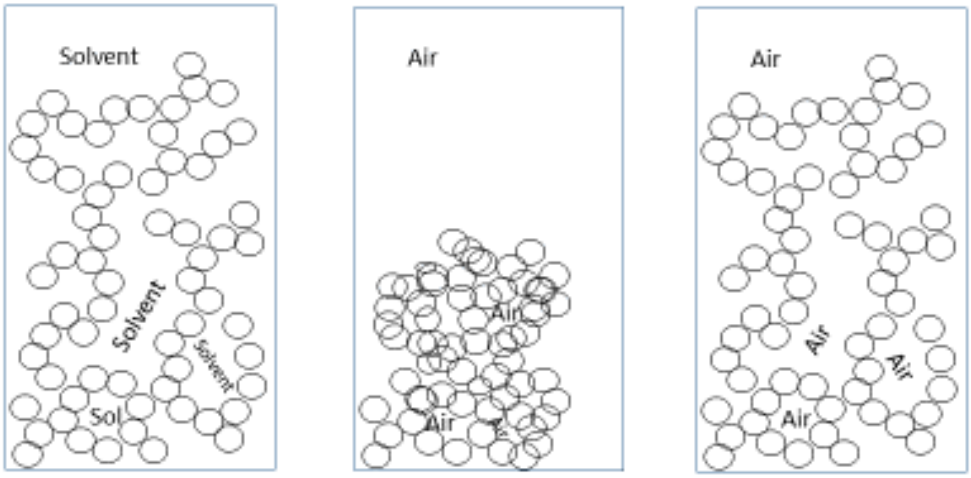

Figure 3: Sketch of a wet-gel (left), xerogel (center), and aerogel (right).

There are various drying methods that can be used to remove the solvent from the pores without causing pore collapse; however, most of these are time consuming. Union College has recently patented a Rapid Supercritical Extraction (RSCE) technique, unique in that it uses a hot press.[5,6] RSCE fabricates aerogels safer and quicker than some other traditional methods, such as the high-temperature extraction of alcohol solvent in an autoclave. The RSCE technique involves pouring the precursor solution in a mold before it condenses into a wet gel, then creating a sealed system by sandwiching the mold between two platens in a hot press. The hot press is used to increase the temperature and pressure on the wet gel until the solvent passes its critical point and becomes a supercritical fluid. At this point there is no surface tension against the pores, and the supercritical fluid safely can leave the system without pore collapse. The solvent-free, porous structure left behind is the aerogel.[7,8] Anderson et al. were able to make transparent, monolithic silica aerogels in under three hours by varying the temperature, temperature rate, and pressure release rate using the RSCE process.[9]

III. Introduction to Chemical Probes

Chemical probes are molecular species that produce a response based on interaction with a change in their environment. There is a history of various types of chemical probes to

---

[5] B. M. Gauthier, A. M. Anderson, S. Bakrania, M. K. Mahony, and R. B. Bucinell. Method and Device for Fabricating Aerogels and Aerogel Monoliths Obtained Thereby. Patent US 7384988 B2. 2008

[6] B. M. Gauthier, A. M. Gauthier, S. D. Bakrania, M. K. Mahony, and R. B. Bucinell, Method and Device for Fabricating Aerogels and Aerogel Monoliths Obtained Thereby. Patent US 8080591 B1. Dec 20 2011.

[7] B. M. Gauthier, S. D. Bakrania, A. M. Anderson, and M. K. Carroll. "A fast supercritical extraction technique for aerogel fabrication." *Journal of Non-Crystalline Solids* 350 (2004): 238-43.

[8] Mary K. Carroll, Ann M. Anderson, and Caroline A. Gorka. "Preparing silica aerogel monoliths via a rapid supercritical extraction method." *JoVE (Journal of Visualized Experiments)*.84 (2014): e51421-.

[9] A. M. Anderson, C. W. Wattley, and M. K. Carroll. "Silica aerogels prepared via rapid supercritical extraction: Effect of process variables on aerogel properties." *Journal of Non-Crystalline Solids* 355.2 (2009): 101-8.

detect oxygen. Early oxygen sensor work used electrode sensors. These measured the reduction of oxygen to detect a current flow.[10] There is also a precedent to incorporate not just oxygen sensors, but other sorts of chemical probes into aerogel materials. Carroll and Anderson give a review of the use of aerogel materials for the incorporation of chemical probes. According to Carroll and Anderson, the high porosity, relatively low density, and optical properties of some sol-gel materials contribute to their use as chemical probes. The nature of silica aerogels as optical sensors and as sensors based on the measurements of conductance are both discussed in the review chapter by Carroll and Anderson.[11] For example, thin films have been doped with $LiNiO_3$ for detecting oxygen through the change in conductivity.[12]

As discussed above, an oxygen sensor is a molecule that produces a response based on the interaction with oxygen in the environment. A chemical probe will respond differently to outside stimuli based on the microenvironment that that probe is in. Sol gels, including wet gels, xerogels and aerogels, have four distinct microenvironments.[13] Dunn and Zink describe these four microenvironments as the region when a dopant molecule is inside the pore, when a dopant molecule is within a few molecular diameters of the pore wall, when the dopant molecule is incorporated into the pore wall, and when the dopant molecule is about the size of the pore itself, and effectively encased. The response that an oxygen-sensitive probe has to the

[10] Leland C. Clark and Champ Lyons. "Electrode systems for continuous monitoring in cardiovascular surgery." *Annals of the New York Academy of Sciences* 102.1 (1962): 29-45.

[11] M. K. Carroll and A.M Anderson. "Aerogels as Platforms for Chemical Sensors." *Aerogels Handbook.* Eds. M. A. Aegerter, N. Leventis, and M. M. Koebel. Springer Science+Business Media, 2011. 637-649.

[12] Lu Xuchen, Xu Tingxian, and Dong Xianghong. "Preparation and characterization of LaNiO3 A/F ratio-sensitive thin film by sol–gel process based on amorphous citrate precursors." *Sensors and Actuators B: Chemical* 67.1–2 (2000): 24-8.

[13] B. Dunn and J. I. Zink. "Probes of Pore Environmental and Molecule-Matrix Interactions in Sol-Gel Materials." *Chemistry of Materials* 9 (1997): 2280-2291.

presence of oxygen differs based on which microenvironment it is located in. Oftentimes this response is in the form of fluorescence, and the sensor is known as an optical oxygen sensor.

IV. Luminescence

Occasionally a photon of energy will impact a molecule. If the photon corresponds to an electronic transition of the molecule, it could cause an electron in the molecule to move from the Highest Occupied Molecular Orbital (HOMO) to the Lowest Unoccupied Molecular Orbital (LUMO). This gain of energy causes the molecule to leave the ground state, usually a singlet state (S_0), and enter an excited state (usually S_1). Some of that energy will then be lost as heat through vibrational energy.[14] The molecule can release the remaining absorbed energy in the form of light as it moves back into the ground state, as the electron goes from the LUMO back to the HOMO. Anytime light is released from a molecule, the process is known as luminescence, and the molecule is known as a luminophore.

Specifically, when this release of energy occurs from an excited state to a ground state of the same multiplicity (such as S_1 to S_0), the release of energy in the form of light is known as fluorescence, and the molecule is known as a fluorophore.[15] Occasionally an excited molecule will undergo a spin conversion, for example moving from the S_1 to a triplet state, T_1. The move from a triplet state to a ground state is forbidden, and as a result a population of molecules will experience luminescence over a longer period of time. This emission is known as

[14] J. R. Lakowicz. "Introduction to Fluorescence." *Principles of Fluorescence Spectroscopy.* 2nd ed. Kluwer Academic/ Plenum Publishers, 1999. 1-20.

[15] J. R. Lakowicz. "Introduction to Fluorescence." *Principles of Fluorescence Spectroscopy.* 2nd ed. Kluwer Academic/ Plenum Publishers, 1999. 1-20.

phosphorescence.[16] The processes of absorbance, fluorescence and phosphorescence are shown in Figure 4.

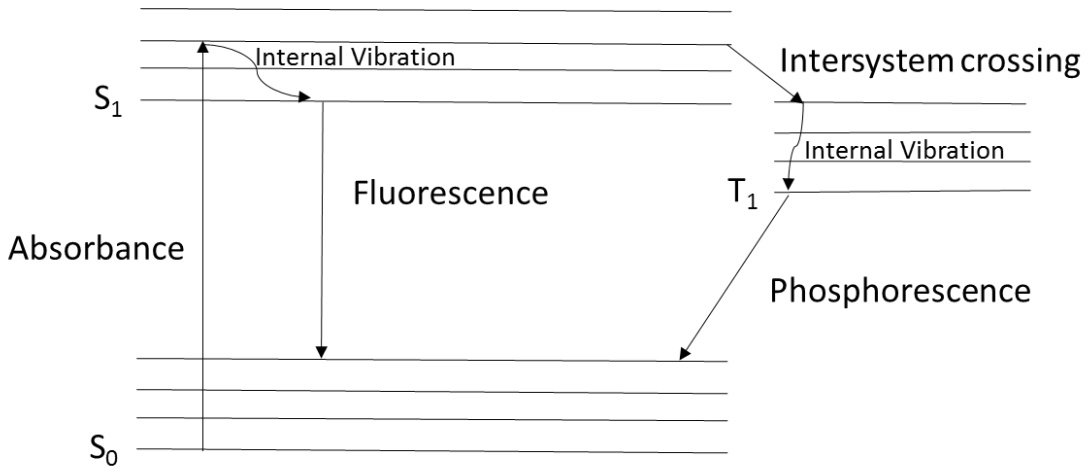

Figure 4: Diagram illustrating molecular electronic transitions. The electronic transitions corresponding to absorbance, internal vibration and fluorescence are displayed as a molecule goes from the ground state, S_0, to the excited state, S_1. Also shown is the intersystem crossing from the excited singled state to the excited triplet state, T_1, and phosphorescence as the molecule undergoes a forbidden transition from the T_1 to S_0 state.

Fluorescence can be inhibited by various processes. When another molecule inhibits a fluorophore, the process is known as fluorescence quenching. For example, when some fluorophores undergo a collision with oxygen, the fluorophore undergoes collisional quenching. Energy is transferred to the oxygen, and the fluorescence intensity is decreased for the system containing the fluorophores.[17] For a single fluorophore in a single microenvironment, the effect

[16] J. R. Lakowicz. "Introduction to Fluorescence." *Principles of Fluorescence Spectroscopy.* 2nd ed. Kluwer Academic/ Plenum Publishers, 1999. 1-20.

[17] J. R. Lakowicz. "Introduction to Fluorescence." *Principles of Fluorescence Spectroscopy.* 2nd ed. Kluwer Academic/ Plenum Publishers, 1999. 1-20.

that the concentration of a quencher can have on the fluorescence intensity of a fluorophore can be determined using the Stern-Volmer equation, shown as equation 1:[18]

$$\frac{F_0}{F} = 1 + K[Q] \qquad \text{Equation (1)}$$

where K is the Stern-Volmer quenching constant, unique to a fluorophore in a particular microenvironment. F_0 is the intensity of the fluorophore in the absence of quencher, [Q] is the concentration of quencher present, and F is the intensity of the fluorophore in the presence of a specific concentration of quencher. Note that since K is unique to the microenvironment a fluorophore is present in, the same fluorophore will have two different K values for two different microenvironments.

Many, but not all, fluorescent oxygen sensors work on this principle. By determining the intensity of a specific fluorophore in the absence of oxygen, and then again with different concentrations of the oxygen, one can determine the Stern-Volmer quenching constant for a fluorophore in a specific microenvironment. Using that and the Stern-Volmer equation, one can then determine an unknown concentration based on the observed decrease in fluorescence intensity.

If a fluorophore is present in more than one microenvironment, then a more complicated version of the Stern-Volmer equation is required to account for the distinct quenching constants. A modified Stern-Volmer equation can be used, which assumes that the

[18] J. R. Lakowicz. "Introduction to Fluorescence." *Principles of Fluorescence Spectroscopy.* 2nd ed. Kluwer Academic/ Plenum Publishers, 1999. 1-20.

probes are present in two different regions, one of which is inaccessible to the quencher. This is shown in equation 2:[19]

$$\frac{F_o}{\Delta F} = \frac{1}{f_a K_a [Q]} + \frac{1}{f_a} \qquad (2)$$

where $F_o/\Delta F$ is the ratio of unquenched luminescence intensity to the change in luminescence intensity in the presence of a quencher, f_a is the fraction of the luminophore available to the quencher, and K_a is the Stern-Volmer quenching constant of the accessible fraction.

Other fits can be used to model the luminophore-probe interaction as well, through the use of modeling programs such as KaleidaGraph. One such other fit is the assumption that the probe is in two distinct microenvironments, each of which is accessible to the quencher. Demas et al. created an equation to fit a Stern-Volmer plot in this situation, which is shown as equation 3:[20]

$$\frac{F_0}{F} = \frac{1}{\frac{f_1}{1+K_{sv1}[Q]} + \frac{f_2}{1+K_{sv2}[Q]}} \qquad (3)$$

where F_o/F is the ratio of unquenched luminescence intensity to quenched luminescence intensity, f_1 and f_2 are the fractions of luminophore available to the quencher in the two microenvironments, and K_{sv1} and K_{sv2} are the Stern-Volmer quenching constants for the fluorophore in each microenviroment.

---

[18] J. R. Lakowicz. "Quenching of Fluorescence." *Principles of Fluorescence Spectroscopy.* 2nd ed. Kluwer Academic/ Plenum Publishers, 1999. 237-261.

[19] J. N. Demas, B. A. DeGraff, and Wenying Xu. "Modeling of Luminescence Quenching-Based Sensors: Comparison of Multisite and Nonlinear Gas Solubility Models." *Analytical Chemistry* 67.8 (1995): 1377-80.

V. Chemical probes in sol-gel materials and sol-gel-related materials

Optical oxygen sensors can be incorporated into materials other than sol gels. Hutter et al. have manufactured optical oxygen sensors that emit in the near infrared (NIR) region. With these oxygen sensors the platinum(II)-benzoporphyrins covalently bond to a polymer matrix either through Suzuki reactions or copolymerization.[21] Metal compounds such as Pt(II) benzoporphyrin (PtBP), and Pd(II) benzoporphyrin (PdBP) have been incorporated into polyphenylenesulfide (PPS) films to serve as optical oxygen sensors for food packaging materials.[22,23]

As for sol gels, there are various ways to incorporate optical sensors into sol-gel materials, specifically silica aerogels. Carroll and Anderson wrote a review chapter that discussed four ways of creating an optical sensor aerogel.[24] In the first, Ayers and Hunt discovered that when silica aerogels were exposed to energized ammonia, serving as a reducing gas, the aerogel itself was modified to be luminescent. However these aerogels were hydrophilic

[21] L. H. Hutter, B.J. Muller, K. Koren, S.M. Borisov, and I. Klimant. "Robust optical oxygen sensors based on polymer-bound NIR-emitting platinum(ii)-benzoporphyrins." *Journal of Materials Chemistry C* 2.36 (2014): 7589-98.

[22] C. A. Kelly, C. Toncelli, M. Cruz-Romero, O. V. Arzhakova, J. P. Kerry, and D. B. Papkovsky. "Phosphorescent O2 sensors integrated in polymeric film materials by local solvent crazing." *Materials & Design* 77 (2015): 110-3.

[23] C. Toncelli, O. V. Arzhakova, A. Dolgova, A. L. Volynskii, J. P. Kerry, and D. B. Papkovsky. "Phosphorescent oxygen sensors produced by spot-crazing of polyphenylenesulfide films." *Journal of Materials Chemistry C* 2.38 (2014): 8035-41.

[24] M. K. Carroll and A. M. Anderson. "Aerogels as Platforms for Chemical Sensors." *Aerogels Handbook.* Eds. M. A. Aegerter, N. Leventis, and M. M. Koebel.Springer Science+Business Media, 2011. 637-649.

and dissolved in contact with water. The hydrophilic aerogels can become hydrophobic through treatment post-fabrication.[25]

The second method of modification discussed was covalently attaching the probe to the backbone of the aerogel. Leventis et al. were able to covalently bond the fluorophore *N*-(3-trimethoxysilylpropyl)-2-7-diazapyrenium bromide (DAP) to the silica atom by mixing a solution of DAP and TEOS before gelation of the sol-gel. This method created aerogels that allowed oxygen to permeate the aerogel matrix near the speed of open-air diffusion.[26] If a sensor can respond at the speed of open-air diffusion, it has an ideal response time. The third method of modification was also by Leventis et al. A silica wet gel was soaked in a fluorophore solution, in this case ruthenium(II) *tris*-(1,10-phenanthroline), and the fluorophore would electrostatically attach itself to the silica backbone.[27] The last method discussed to modify the silica aerogels was by Plata et al., and involved mixing the fluorophore with the initial sol-gel precursor mixture before gelation. The RSCE drying method was then used to remove the solvent, trapping the fluorophore inside the pores of the aerogels.[28] This is the approach taken in this thesis.

---

[25] Michael R. Ayers and Arlon J. Hunt. "Molecular oxygen sensors based on photoluminescent silica aerogels." *Journal of Non-Crystalline Solids* 225 (1998): 343-7.

[26] N. Leventis, I. A. Elder, D. R. Rolison, M. L. Anderson, and C. I. Merzbacher. "Durable Modification of Silica Aerogel Monoliths with Fluorescent 2,7-Diazapyrenium Moieties. Sensing Oxygen near the Speed of Open-Air Diffusion." *Chemistry of Materials* 11 (1999): 2837-2845.

[27] N. Leventis, A. M. Rawashdeh, I. A. Elder, J. Yang, A, and C. Sotiriou-Leventis. "Synthesis and Characterization of Ru(II) Tris(1,10-phenanthroline)-Electron Acceptor Dyads Incorporating the 4-Benzoyl-N-methylpyridinium Cation or N-Benzyl-N'-methyl Viologen. Improving the Dynamic Range, Sensitivity, and Response Time of Sol-Gel-Based Optical Oxygen Sensors." *Chemistry of Materials* 16.8 (2004): 1493-506.

[28] D. L. Plata, Y. J. Briones, R. L. Wolfe, M. K. Carroll, S. D. Bakrania, S. G. Mandel, and A. M. Anderson. "Aerogel-platform optical sensors for oxygen gas." *Journal of Non-Crystalline Solids* 350 (2004): 326-35.

There are many factors that can be used to tune the physical properties of a sol-gel matrix. Huang et al. found they could use a drying control chemical additive (DCCA) to tune the size and shape of pores in the sol-gel matrix.[29] They used formamide to create larger pores in silica films. Doing this allowed oxygen to flow more easily past their ruthenium-based sensor ($Ru(bpy)_3^{2+}$). A sensor's response to oxygen can also be optimized based on the initial recipe used to make the sol-gel mixture. McEvoy et al. determined that varying the ratio of precursor to water in the sol-gel mixture can optimize the sensor's response to oxygen.[30]

Previous researchers at Union College have incorporated fluorescent oxygen sensors into silica aerogels. Some of these include tris(2,2'-bipyridyl)ruthenium(II) ($Ru(bpy)_3^{2+}$), ruthenium(II)4,7-diphenyl-1,10-phenanthroline ($Ru(dpp)_3^{2+}$), and platinum(II) octaethylporphyrin (PtOEP). It was determined in these studies that the fluorophore was entrapped within the aerogel matrix as it formed. The observed change in fluorescence intensity due to oxygen quenching was both rapid and reversible for these fluorophores in silica aerogels.[31]

Other work from the Union College Aerogel Lab has shown that sonicating the sol-gel solution before gelation sets in gives the resulting aerogel a higher intensity of fluorescence than does manual stirring before gelation.[32] However, initial work that has been performed on

[29] J. Huang, Y. Han, F. Y. Yue, and D. S. Jiang. "Sol-gel Derived Complex Sensing Membranes for Detection of Oxygen." *Key Engineering Materials* 249 (2003): 421-4.

[30] A. K. McEvoy, C. McDonagh, and B. D. MacCraith. "Optimisation of Sol-Gel-Derived Silica Films for Optical Oxygen Sensing." *Journal of Sol-Gel Science and Technology* 8.1-3 (1997): 1121-5.

[31] D. L. Plata, et al. "Aerogel-Platform Optical Sensors for Oxygen Gas." 350 (2004): 326-335.

[32] A. F. Phillips, Fabrication and Characterization of PtOEP-doped Silica Aerogels with Varied Amounts of Water for Use as Oxygen Sensors, Bachelors in Chemistry; thesis, Union College, 2006, 1-37.

PtOEP-doped silica aerogels indicate that those aerogels have diminishing fluorescence ratios after multiple scans with varying oxygen flow.[33]

A study by Reichbind demonstrated that the high temperature involved with the RSCE process thermally degrades potential probes, limiting the options available for optical oxygen sensors.[34] That study indicated that Eosin Y was a functional fluorophore at moderate concentrations. However, it underwent thermal degradation at low concentrations and was too opaque at high concentrations for significant fluorescence measurements. Rhodamine B, Rhodamine 6G, and Fluorescein all exhibited fluorescence emission spectra, indicating that they survived the RSCE process. A potential change in their fluorescence intensity upon exposure to oxygen has yet to be tested. However, Kahn et al. has demonstrated that Rhodamine 6G does not produce a response to oxygen concentration.[35]

VI: Fluorescence Imaging Techniques

Fluorescence can be useful for more than just determining the concentration of a compound. Other fluorescence techniques include fluorescence recovery after photobleaching (FRAP), fluorescence correlation spectroscopy (FCS), and confocal scanning laser fluorescence microscopy (CSLM). FRAP can be used to study the mobility of biological macromolecules in

[33] A. F. Phillips, Fabrication and Characterization of PtOEP-doped Silica Aerogels with Varied Amounts of Water for Use as Oxygen Sensors, Bachelors in Chemistry; thesis, Union College, 2006, 1-37.

[34] J. R. Reichbind, Suitability of Silica Aerogels as Platforms for Sensors Based on Phosphorescent Probes, Bachelors in Chemistry; thesis, Union College, 2007, 1-55.

[35] A. Kahn, F. Wang, Y. Raval, T. R. Tzeng, and J. Anker. "Fabrication of Oxygen-Sensor Films for Detecting and Treating Infections." Interfaces and Surfaces NSF REU Site (2013), https://www.ces.clemson.edu/mse-reu/wp-content/uploads/2014/08/Kahn.pdf

membranes.[36] FCS can be used to determine interactions of fluorescent biomolecules in systems ranging from cells to whole organisms, measuring intensity fluctuations by a stream of molecules coursing through a sub-µm detection volume.[37] CSLM can be used to determine crystalline structures of particles. For example, Van Blaaderen et al. were able to image colloidal particles in three dimensions.[38]

VII: Project Goals

The goal of this project is to investigate if it is possible to observe changes in fluorescence signal in relation to oxygen traveling through a silica aerogel monolith. Challenges include spatial and temporal resolution. A long-range goal is to investigate if it is possible to create a spectroscopic in-situ measurement of oxygen concentration while in the Union Catalytic Aerogel Testbed (UCAT) system. Initial tests so far have looked into Rhodamine 6G and PtOEP. Rhodamine 6G (R6G) and Platinum (II) Octaethylporphyrin (PtOEP) are both luminophores. R6G is displayed in Figure 5 and PtOEP in Figure 6.

[36] J. Davoust, P. F. Devaux, and L. Leger. "Fringe pattern photobleaching, a new method for the measurement of transport coefficients of biological macromolecules." *The EMBO journal* 1.10 (1982): 1233-8.

[37] J. Ries and P. Schwille. "Fluorescence correlation spectroscopy." *BioEssays* 34.5 (2012): 361-8.

[38] A. Van Blaaderen, A. Imhof, W. Hage, and A. Vrij. "Three-dimensional imaging of submicrometer colloidal particles in concentrated suspensions using confocal scanning laser microscopy." *Langmuir* 8.6 (1992): 1514-7.

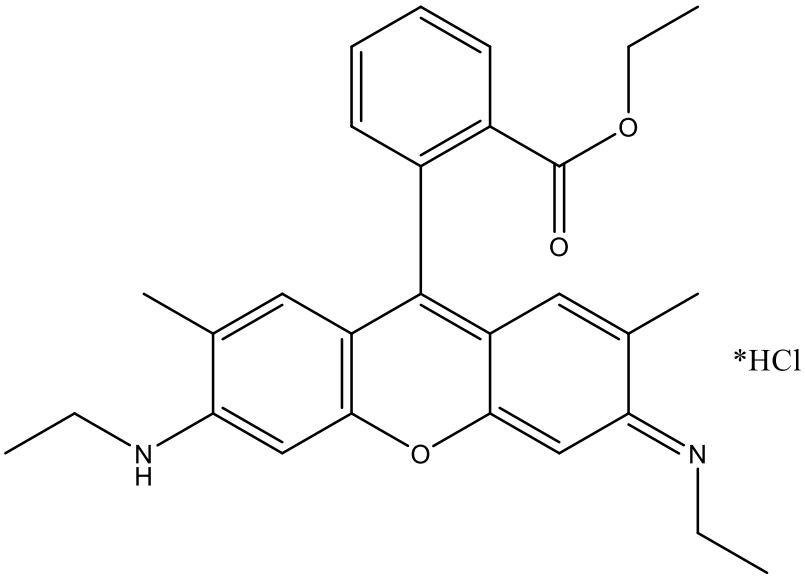

Figure 5: Chemical structure of Rhodamine 6G.

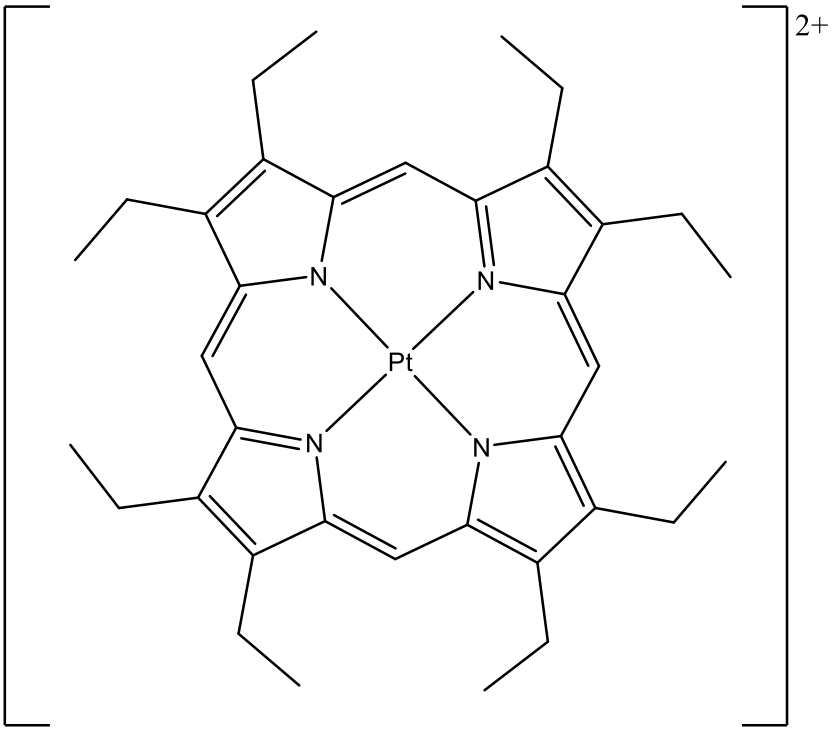

Figure 6: Chemical structure of Platinum (II) Octaethylporphyrin.

Experimental

I. Fabrication of Aerogels and Xerogels

Tetramethyl orthosilicate (TMOS) of 98% purity was acquired from Sigma-Aldrich. Rhodamine 6G (R6G), ~95% purity, was acquired from Sigma-Aldrich. Platinum (II) octaethylporphyrin (PtOEP) was acquired from Frontier Scientific. Ammonia solutions were made by dilution of concentrated ammonia from Fisher Scientific with in-house deionized water. Methanol (≥ 99.8% purity) was also acquired from Fisher Scientific. All reagents were used without further purification.

All aerogels and xerogels were fabricated using a recipe listed in Table I that was adapted from the Standard TMOS recipe.[39]

Table 1: TMOS recipe employed for gel fabrication

Precursor	**Volume (mL)**
Tetramethyl orthosilicate (TMOS)	8.5
Methanol	27.5
Deionized water	3.6
1.5 M NH_3	0.270

[39] A. F. Phillips, Fabrication and Characterization of PtOEP-doped Silica Aerogels with Varied Amounts of Water for Use as Oxygen Sensors, Bachelors in Chemistry; thesis, Union College, 2006, 1-37

For various batches of aerogels, this recipe was scaled up to different total volumes. For all recipes, the volumetric ratios between the precursors stayed the same. This volumetric ratio between the precursors is displayed in Table 2.

Table 2: TMOS recipe volume ratio	
Precursor	**Volume Ratio**
TMOS	1.00
Methanol	3.24
Deionized water	0.42
1.5 M NH_3	0.0318

For all of the luminescent-probe-doped aerogels manufactured, the ratio in Table 2 was followed, with the methanol being substituted by an equivalent volume of solution of the probe in methanol or a combination of probe in methanol and methanol. Aerogel batches that had left-over solution were used to make the corresponding batches of xerogels.

A 1.00×10^{-3}-M Rhodamine 6G (R6G) solution was prepared by mixing 47.9 mg of R6G in a 100-mL volumetric flask with methanol. The other R6G solutions were created from serial dilutions of this initial 10^{-3} M R6G solution with methanol.

A 3×10^{-5}-M platinum(II) octaethylporphyrin (PtOEP) was created by measuring 0.02 g of PtOEP into a 1-L volumetric flask and diluting to the line with methanol. The other PtOEP solutions were created from serial dilutions of this initial 3×10^{-5} M PtOEP solution with methanol. The PtOEP was not very soluble, so the flask had to be shaken to attempt to homogenize the "3×10^{-5} M" solution before any serial dilution was performed. It is likely that the concentrations of the PtOEP solutions are actually lower than what they are reported as here, due to the solubility issues.

Note that while all the aerogels were prepared using an optical sensor solution of established concentration, the concentration of sensor in the aerogel was not definitively known, since the sensor solution was mixed with other precursors, and then some of the probe molecules could have decomposed during the hot press procedure. In this thesis, an aerogel made using a specific concentration of optical sensor solution, will be referred to as an aerogel with that concentration of sensor (for example, an aerogel made using the $1x10^{-5}$ M R6G solution will be referred to as a "10^{-5}-M R6G" aerogel).

Luminescent-probe-doped xerogels followed the ratio listed in Table 2. However an optical sensor solution in methanol replaced the pure methanol for each batch. Similar to the aerogels, while all the xerogels were created using an optical sensor solution, the concentration of sensor in the xerogel was not definitively known, since the sensor solution was mixed with other precursors, and then the solution was dried at room temperature where some of the pores collapsed. This resulted in a decrease in volume and potential increase in sensor concentration. In this thesis, a xerogel made using a specific concentration of optical sensor solution, will just be referred to as a xerogel with that concentration of sensor (for example, a xerogel made using the $1x10^{-5}$ M R6G solution will be referred to as a "10^{-5}-M R6G" xerogel).

For all sol-gel solutions, the precursors were mixed together in a glass beaker, then covered with Parafilm and sonicated for 10 minutes. A list of all Rhodamine 6G aerogel and xerogel batches can be found in Table 3. A list of all Platinum (II) Octaethylporphyrin aerogel and xerogel batches can be found in Table 4. Table 5 is a list of aerogels and xerogels that included both probes.

Table 3: Rhodamine 6G (R6G) Aerogels and Xerogels			
Aerogels		**Xerogels**	
Batch Name	Methanol Substitute	Batch Name	Methanol Substitute
R6G-A-01[1]	10^{-4} M R6G	R6G-X-01	10^{-4} M R6G
		R6G-X-02[1]	10^{-4} M R6G
		R6G-X-03	10^{-5} M R6G
		R6G-X-04	10^{-5} M R6G
R6G-A-02[2]	10^{-4} M R6G	R6G-X-05	10^{-6} M R6G
		R6G-X-06	10^{-5} M R6G
		R6G-X-07	10^{-6} M R6G
		R6G-X-08[2]	10^{-6} M R6G
Note: Aerogel and xerogel batches with the same numerical superscript were made from the same initial batch of solution			

Table 4: Platinum (II) Octaethylporphyrin (PtOEP) Aerogels and Xerogels			
Aerogels		**Xerogels**	
Batch Name	Methanol Substitute	Batch Name	Methanol Substitute
PtOEP-A-01[1]	10^{-6} M PtOEP	PtOEP-X-01[1]	10^{-6} M PtOEP
PtOEP-A-02[2]	10^{-5} M PtOEP	PtOEP-X-02[2]	10^{-5} M PtOEP
PtEOP-A-03	10^{-5} M PtOEP*	PtOEP-X-03	10^{-5} M PtOEP*
PtOEP-A-04	$3x10^{-5}$ M PtOEP	PtOEP-X-04	10^{-5} M PtOEP*
PtOEP-A-05[3]	$3x10^{-5}$ M PtOEP	PtOEP-X-05	10^{-5} M PtOEP*
PtOEP-A-06[4]	$3x10^{-5}$ M PtOEP	PtOEP-X-06[3]	$3x10^{-5}$ M PtOEP
PtOEP-A-07	$3x10^{-5}$ M PtOEP	PtOEP-X-07[4]	$3x10^{-5}$ M PtOEP
Note: Aerogel and xerogel batches with the same numerical superscript were made from the same initial batch of solution. * = Instead of using 10^{-5} M stock solution, made methanol substitute from $3x10^{-5}$ M stock solution diluted in methanol.			

Table 5: Mixed PtOEP-R6G Aerogels and Xerogels		
Batch Name	Methanol Substitute	Volume (mL)
Mix-A-01 Mix-X-01	10^{-5} M R6G	2.75
	$2.75x10^{-5}$ M PtOEP	1
	Methanol	23.75

II. Rapid Supercritical Extraction Process (RSCE)

After the sol-gel mixture was sonicated for 10 minutes, it was ready to go into the hot press. Initially, aerogels were made using a 125 x 125 x 12 mm mold, with 16 cylindrical wells, each 9 mm in diameter. Each well had a volume of 0.763 mL, for a total volume of 12.2 mL. The mold was originally designed by Aaron Phillips (’06), Andrew Dikan (’06), and David Korim (’06).[40] This mold is pictured in Figure 7.

The process was designed to have the precursor solution gel within the sealed mold, the solvent inside the sol-gel become a supercritical fluid, and then, when the pressure is released, that supercritical fluid leaves the sol-gel and is vented above the upper platen of the hot press. Since the supercritical fluid has no tension on the pore walls, the structure of the aerogel does not collapse through the process, and what remains is the aerogel monolith.

To manufacture aerogels that had a snug fit in cuvettes to facilitate optical measurements, a new mold was designed with help from Elizabeth Donlon (’18). The mold is 127 x 127 x 12.7 mm, with 16 rectangular-prism wells. Each of the wells is 10 x 10 mm wide, with a height 12.7 mm, for a volume of 1.27 mL per well, and a total volume of 20.3 mL. This mold is pictured in Figure 8.

[40] A. F. Phillips, Fabrication and Characterization of PtOEP-doped Silica Aerogels with Varied Amounts of Water for Use as Oxygen Sensors, Bachelors in Chemistry; thesis, Union College, 2006, 1-37.

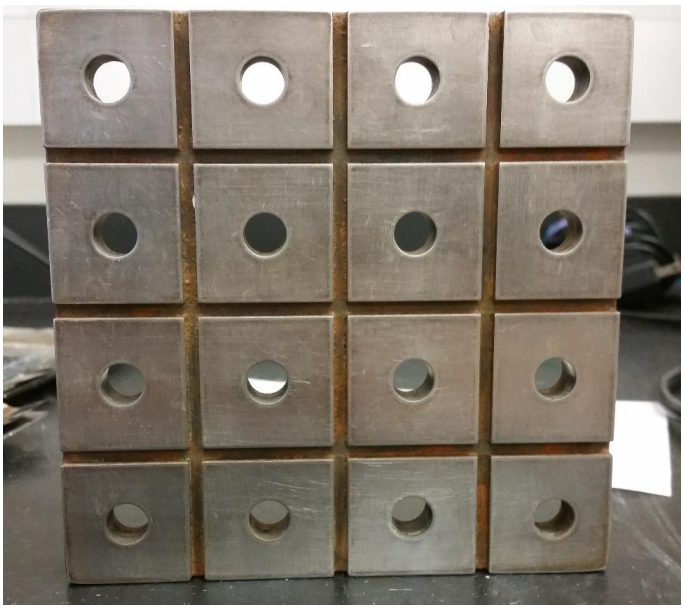

Figure 7: 125 x 125 x 12.5 mm mold, with 16 wells, each 9 mm wide.

Figure 8: 127 x 127 x 12.7 mm mold, with 16 wells, each 10 x 10 x 12.7 mm.

The mold was sandwiched between two sheets of 0.0005” stainless steel, which were respectively sandwiched between two sheets of 1/16” graphite. Before the hot press procedure

to fabricate the aerogels was performed, the mold was sprayed with dry lubricant, to make retrieval of the aerogels easier post fabrication. Sprayon LU708 and CRC Industrial Dry PTFE Lube were used interchangeably as the dry lubricant. In order to seal the bottom of the mold, so the sol-gel precursor solution would not leak out, a sealing procedure was performed on the mold. For this, the mold underwent 89 kN of force (20.0 kips) for 10 minutes. For later batches, the sealing force was raised to 111 kN of force (25.0 kips) for 10 minutes.

After the mold was sealed, a liquid sol-gel mixture was added to the empty wells using a disposable glass pipet. Leftover solution was poured into 10 x 10 x 45 mm polystyrene plastic cuvettes, and capped to allow gelation to take place. After gelation, the cuvettes were uncapped to allow drying into xerogels.

Once the wells in the mold were filled, a five-step rapid supercritical extraction (RSCE) aerogel fabrication procedure was performed.[41,42,43] Three different processes were used over the course of this thesis for the 16-well molds. The first employed, displayed in Table 6, are those specified by Backlund.[44] All R6G batches were manufactured using the parameters in

[41] B. M. Gauthier, A. M. Anderson, S. D. Bakrania, and M. K. Carroll, "A fast supercritical extraction technique for aerogel fabrication." *Journal of Non-Crystalline Solids* 350 (2004): 238-43.

[42] B. M. Gauthier, A. M. Anderson, S. D. Bahrania, M. K. Mahony, and R. B. Bucinell, Method and Device for Fabricating Aerogels and Aerogel Monoliths Obtained Thereby. Patent US 7384988 B2. 2008.

[43] B. M. Gauthier, A. M. Gauthier, S. D. Bakrania, M. K. Mahony, and R. B. Bucinell, Method and Device for Fabricating Aerogels and Aerogel Monoliths Obtained Thereby. Patent US 8080591 B1. Dec 20 2011.

[44] C. J. Backlund, Luminescent Probes of Hydrophobic Silica Aerogels, Bachelors in Chemistry thesis, Union College, 2009, 1-63.

Table 6. Batches PtOEP-A-1 through PtOEP-A-3 and Mix-A-1 were also fabricated with these parameters.

Table 6: Initial hot press parameters for the fabrication of optical-sensor-doped aerogels					
Step	**1**	**2**	**3**	**4**	**5**
Temp (°C)	33 (90 °F)	266 (510 °F)	266 (510 °F)	37.8 (100 °F)	end
Temp Rate (°F/min)	3	3	3	3	end
Force (kN)	125 (28 kips)	125 (28 kips)	4.45 (1 kip)	4.45 (1 kip)	end
Force rate (kN/min)	4.45 (1 kip/min)	4.45 (1 kip/min)	4.45 (1 kip/min)	4.45 (1 kip/min)	end
Dwell Time (min)	2	30	10	1	end

A second set of hot press parameters were also employed, with a higher restraining force. These parameters are displayed in Table 7. The first batch of aerogels manufactured with the parameters in Table 7 was PtOEP-A-4.

Table 7: Second set of hot press parameters for the fabrication of optical-sensor-doped aerogels.					
Step	**1**	**2**	**3**	**4**	**5**
Temp (°C)	33 90 (°F)	266 510 (°F)	266 510 (°F)	37.8 100 (°F)	end
Temp Rate (°F/min)	3	3	3	3	end
Force (kN)	156 (35 kips)	156 (35 kips)	4.45 (1 kip)	4.45 (1 kip)	end
Force rate (kN/min)	4.45 (1 kip/min)	4.45 (1 kip/min)	4.45 (1 kip/min)	4.45 (1 kip/min)	end
Dwell Time (min)	2	30	10	1	end

A third set of parameters were established with a lower maximum temperature. These parameters are in Table 8. Batches PtOEP-A-5 and PtOEP-A-6 were manufactured using the parameters in Table 8.

Table 8: Modified hot press parameters for the fabrication of optical sensor doped aerogels.

Step	**1**	**2**	**3**	**4**	**5**
Temp (°C)	33 90 (°F)	260 500 (°F)	260 500 (°F)	37.8 100 (°F)	end
Temp Rate (°F/min)	3	3	3	3	end
Force (kN)	156 (35 kips)	156 (35 kips)	4.45 (1 kip)	4.45 (1 kip)	end
Force rate (kN/min)	4.45 (1 kip/min)	4.45 (1 kip/min)	4.45 (1 kip/min)	4.45 (1 kip/min)	end
Dwell Time (min)	2	30	10	1	end

A 3.5 x 3.5 x 0.5“ aerogel monolith containing PtOEP, was also manufactured (Batch PtOEP-A-7). This batch used hot press parameters established by Bhuiya et al,[45]shown below in Table 9.

[45] M. M. H. Bhuiya, A. M. Anderson, M. K. Carroll, B. A. Bruno, J. L. Ventrella, B. Silberman and B. Keramati. “Preparation of monolithic silica aerogel for fenestration applications: scaling up, reducing cycle time and improving performance.” *Industrial & Engineering Chemistry Research*, in press.

Table 9: Hot press parameters for the fabrication of larger optical-sensor-doped aerogel monolith.					
Step	**1**	**2**	**3**	**4**	**5**
Temp (°C)	32 90 (°F)	288 550 (°F)	288 550 (°F)	32 90 (°F)	end
Temp Rate (°F/min)	200	4	-	4	end
Force (kN)	200 (45 kips)	200 (45 kips)	4.45 (1 kip)	4.45 (1 kip)	end
Force rate (kN/min)	2669 (600 kip/min)	-	4.45 (1 kip/min)	-	end
Dwell Time (min)	30	55	1	1	end

III. Characterization of aerogels and xerogels

The fluorescence emission spectra of the aerogel and xerogel samples were measured using a PTI Quantamaster Fluorometer with a xenon arc lamp. Unless otherwise noted, all emission spectra were corrected, and single measurements were taken at integration time 0.5 s, and step size 1 nm.

Most samples containing just R6G as a fluorophore were excited at 465 nm, and emission spectra were taken from 500 to 700 nm. Most samples containing PtOEP as a luminophore were excited at 533 nm, and the emission spectra were taken from 550 to 700 nm. Occasionally, the excitation wavelength was varied to determine if a peak in the spectrum was due to luminescence or scattering. It will be noted in the Results if the excitation wavelength was not 465 nm for R6G or 533 nm for PtOEP.

Preliminary work to determine the oxygen sensitivity of the samples consisted of a nitrogen purge. For this nitrogen purge, a disposable glass pipet was attached to the end of a Tygon tube on a nitrogen tank. The nitrogen tank was turned on, the cap of a cuvette containing a sample lifted up just enough to insert the tip of the glass pipet into the opening. A steady, weak flow of N_2 then entered the cuvette, displacing the air. For most samples, the pipet was removed after 30 seconds and the cuvette was quickly capped. A fluorescence emission spectrum was taken with the same parameters as the sample before the N_2 purge for comparison purposes. After the scan, the cap of the cuvette was removed for 30 seconds for most samples to allow the environment inside the cuvette to come to equilibrium with the air in the room, and then the sample was recapped and another emission spectrum was taken for comparison.

Subsequently, Tygon tubing was employed to feed nitrogen from the N_2 tank directly into a cuvette cap in the fluorometer. With this rig, emission scans were taken under ambient conditions, and also under constantly flowing N_2 conditions, at which it was assumed oxygen would have been flushed from inside the sample. Time-based emission scans were performed, in which PtOEP samples were excited with 533 nm light, and the intensity of emission over a period of time was monitored as the N_2 flow was turned on and off to create oxygen-free environments and environments with about 21 % oxygen (ambient conditions). This N_2 tank-fluorometer rig is displayed in Figure 9. The inlet and outlet tubing connected to the cuvette cap in the fluorometer is displayed in Figure 10.

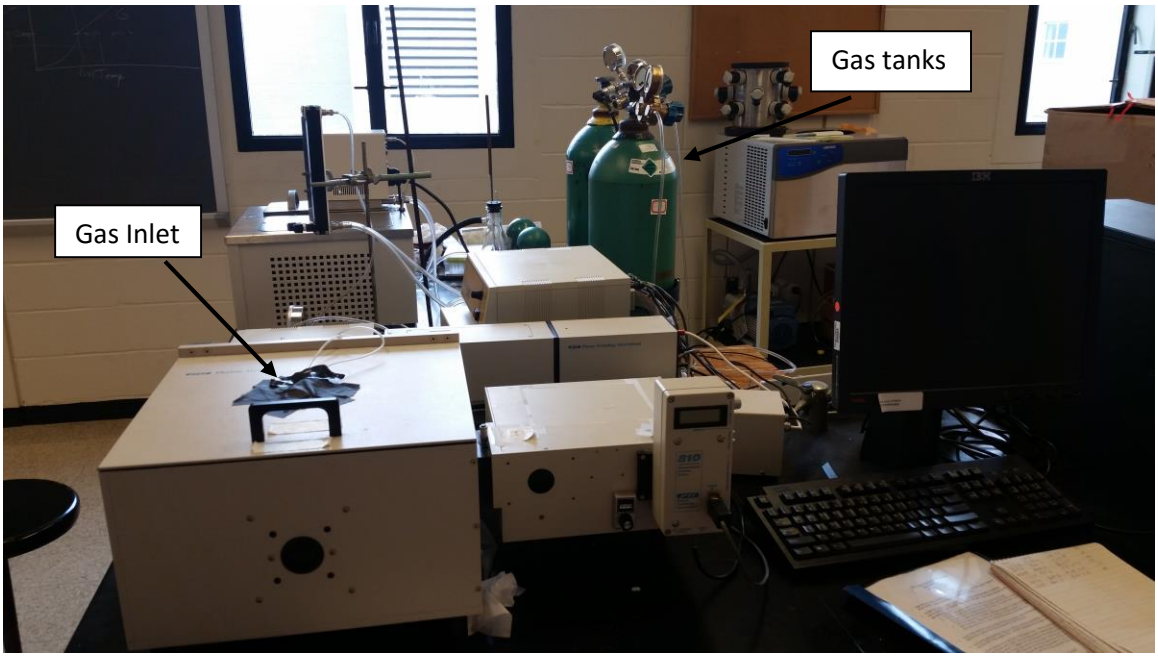

Figure 9: N_2 tank feeding directly into the PTI Quantamaster Fluorometer for oxygen-free emission spectra and time-based scans.

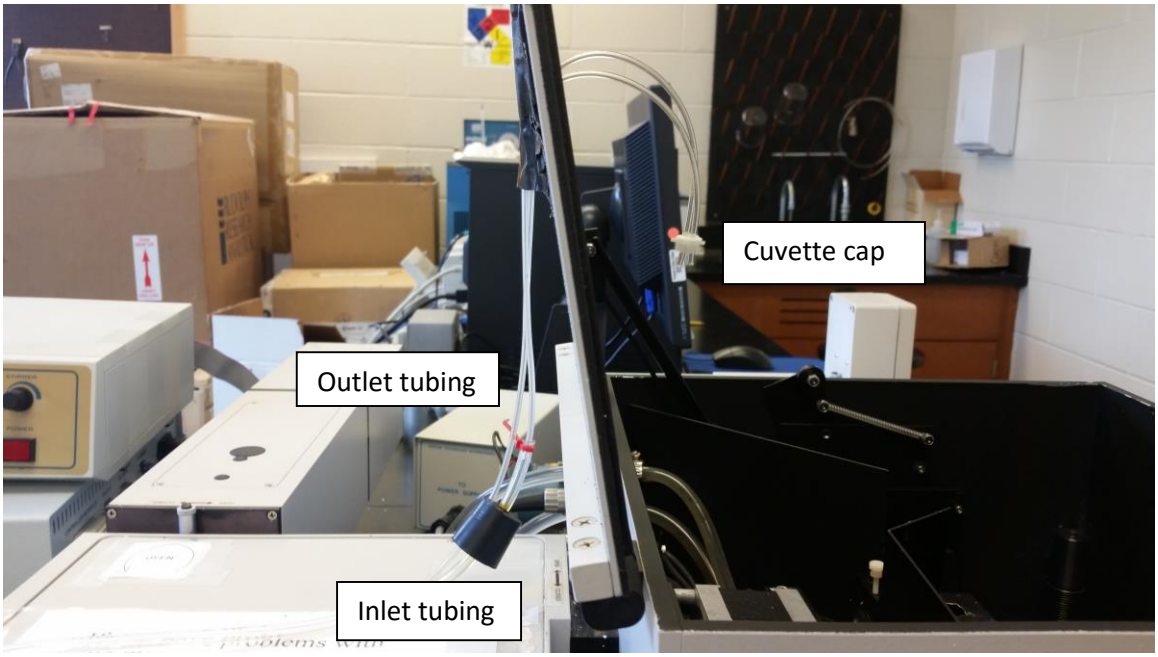

Figure 10: Tubing connected to cuvette cap for fluorometer measurements.

To determine the luminescence of the probes at concentrations of oxygen other than 0 % and 21 % (air), a second gas tank was added to the fluorometer rig which contained an

O_2/N_2 blend. This gas blend was 5.025 mol% O_2 with the remainder being N_2. A gas blend tank that was 0.53% O_2 with the remainder being N_2 and trace amounts of other gases present in air was also used. The N_2 tank and one of the gas blend tanks were connected with Tygon tubing to a gas proportioner system (PMM2-010038, S/N: 93787-1), which connected directly to a sample cuvette cap in the fluorometer. The gas proportioner is displayed in Figure 11.

Figure 11: Left- Front of gas proportioner. The left knob controls the flow rate of N_2, while the right knob controls the flow rate of the gas blend being used. Right- Side view of gas proportioner. The two tubes at the base are the inlet tubes from the N_2 and gas blend tank. The tube at the top is the outlet tube for the proportioned gas.

Scale readings on the gas proportioner represent flow rates for either gas. By varying the scale readings for each gas, the concentration of oxygen could be tuned. Table 10 contains the scale reading to flow rate conversion.[46]

Table 10: Gas Proportioner Calibration Data	
Scale Reading	**Flow (mL/min)**
150	4562
140	4328
130	4101
120	3822
110	3549
100	3294
90	3041
80	2734
70	2419
60	2103
50	1801
40	1497
30	1172
20	828
10	460
0	0

The percentage of oxygen in the gas can be determined with equation 4

$$[O_2] = \frac{5.025 r_{gas}}{r_{gas} + r_{N_2}} \qquad (4)$$

In equation 4, r_{gas} is the flow rate for the gas blend tank, and r_{N_2} is the flow rate for the N_2 tank. This yielded the mole percentage of oxygen in the mixed gas. Each time-based scan

[46] Flowmeter Calibration Data, Document No. 581, Cole Parmer Flowmeter.

would start out with the cuvette in the fluorometer with no flowing gas (ambient conditions), then with just N_2, to create an oxygen-free environment. The concentration of oxygen was then changed in a stepwise fashion by increasing the flow rate of the gas blend and decreasing the flow rate of the N_2. The usual flow rates and times are shown in Tables 11 and 12.

Table 11: Blend Ratios using 5.025% O_2 tank					
Time	**N_2 Scale**	**Flow (mL/min)**	**Blend Scale**	**Flow (mL/min)**	**% O2**
0	0	0	0	0	
60	50	1801	0	0	0.0
300	45	1649	5	230	0.62
400	40	1497	10	460	1.18
500	30	1172	20	828	2.08
600	20	828	30	1172	2.94
700	10	460	40	1497	3.84
800	0	0	50	1801	5.03
900	0	0	0	0	0.0

Table 12: Blend Ratios using 0.53% O_2 tank					
Time	**N_2 Scale**	**Flow (mL/min)**	**Blend Scale**	**Flow (mL/min)**	**% O2**
0	0	0	0	0	
60	50	1801	0	0	0.0
300	45	1649	5	230	0.06
400	40	1497	10	460	0.12
500	30	1172	20	828	0.22
600	20	828	30	1172	0.31
700	10	460	40	1497	0.41
800	0	0	50	1801	0.53
900	0	0	0	0	0.0

Stern-Volmer plots were created by plotting the ratio of the quencher-free luminescence to the luminescence at a specific concentration of quencher, against that concentration of quencher for various samples, following equation 1. The intensities of luminescence at varying quencher concentrations were determined by averaging the

luminescence intensity for the last 20 s measured for each concentration of oxygen. Modified Stern-Volmer plots were created by plotting the ratio of the quencher-free luminescence to the difference of the quenched and quencher-free luminesce, against the inverse of the concentration of quencher for various samples, following equation 2.

Kaleidagraph was used to model a two-site fit to the Stern-Volmer plots. For this, the fractional accessibility and K_{sv} values from the modified Stern-Volmer equations served as initial estimates for the fractional accessibility and K_{sv} of one site, and a value one thousandth of the K_{sv} from the modified Stern-Volmer plots served as the initial estimate for the K_{sv} of the second site.

IV. Monolithic Testing Rig

A proof-of-concept rig was created to see if the fluorescence response of large PtOEP-doped monoliths to oxygen could be visually observed. For this, a clear plastic case with internal dimensions of 5.5 x 4.25 x 1.125” was used to hold a monolithic sample. A 3/10” hole was bored in the middle of either 4.25” side by Paul Tompkins in the Union College Engineering Machine Lab, and Tygon tubing was inserted in both holes to use as a gas inlet and outlet. The case with Tygon tubing is seen in Figure 12. After the cracked 3.5 x 3.5 x 0.5“ aerogel monolith was placed in the case, a layer of Parafilm was wrapped around the lid-case interface, to attempt to eliminate airflow exchanging to and from the case from anywhere other than the inlet and outlet ports.

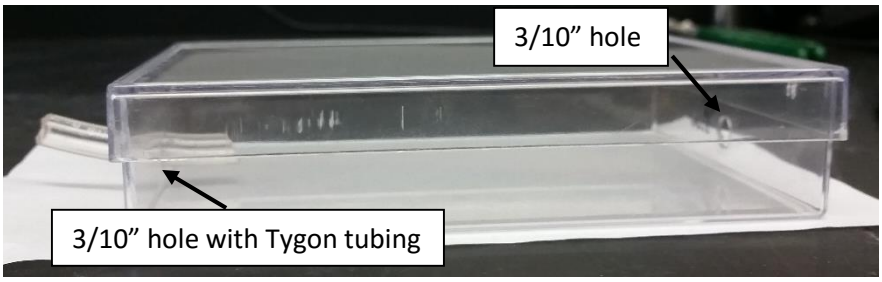

Figure 12: Proof-of-concept sample case with holes bored for inlet and outlet of gas.

A 532-nm laser pointer (Wicked lasers core, S/N A22225) was borrowed from Prof. James McGarrah, and a 520-540 nm laser pointer (Infiniter LR16GR) was borrowed from Prof. Andrew Huisman to be used as excitation sources. Laser goggles that filtered out 532 nm light were borrowed from both Prof. Ann Anderson (Laser Gard Argon) and Prof. Andrew Huisman (uvex VDO laser Eyewear LOTG-ARGON/KTP). The sample was then excited with one of the two laser pointers and observed through the laser goggles both in ambient conditions, and as N_2 was introduced to the sample container.

Results & Discussion

I. Rhodamine 6G

R6G Wet Gels & Xerogels

Upon excitation at 465 nm, all R6G-doped wet gels had fluorescence emission peaks centered around 550 nm, regardless of concentration (10^{-4}, 10^{-5}, and 10^{-6}-M). Figure 13 is the overlaid emission spectra for 10^{-5}-M R6G wet gels. Other concentrations of R6G wet gels (10^{-4} and 10^{-6}-M), exhibited similar emission spectra.

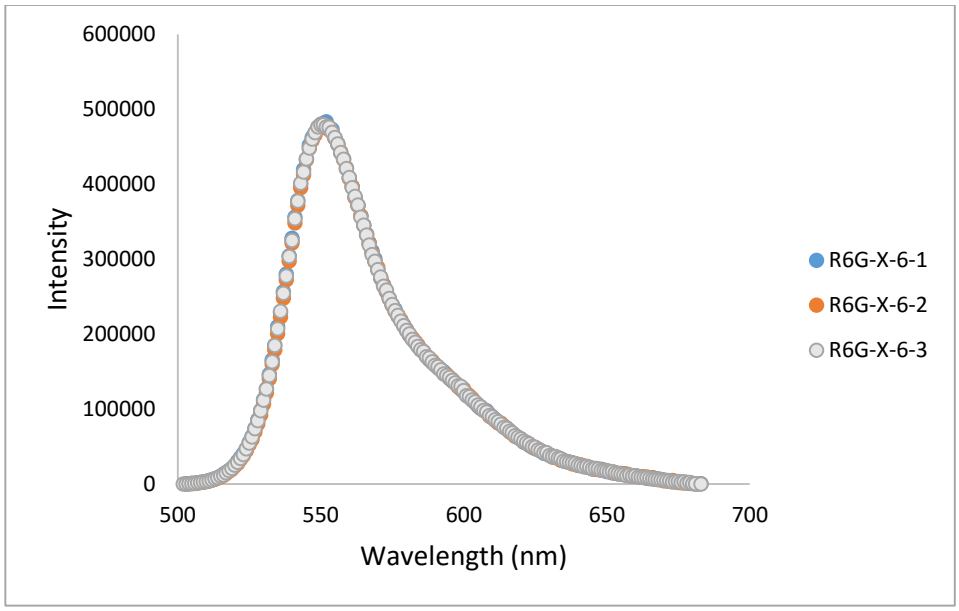

Figure 13: Overlaid emission spectra for three 10^{-5}-M R6G wet-gel samples from batch R6G-X-6, excited at 465 nm, with 1-nm emission and excitation slits.

However, as the wet gels dried, the homogeneity among samples in each batch started to diminish. Figure 14 is the overlaid emission spectra for 10^{-6}-M R6G gels that have dried for at least three days, exhibiting almost xerogel-like physical characteristics by shrinking down to between a fourth and a sixth of their initial size.

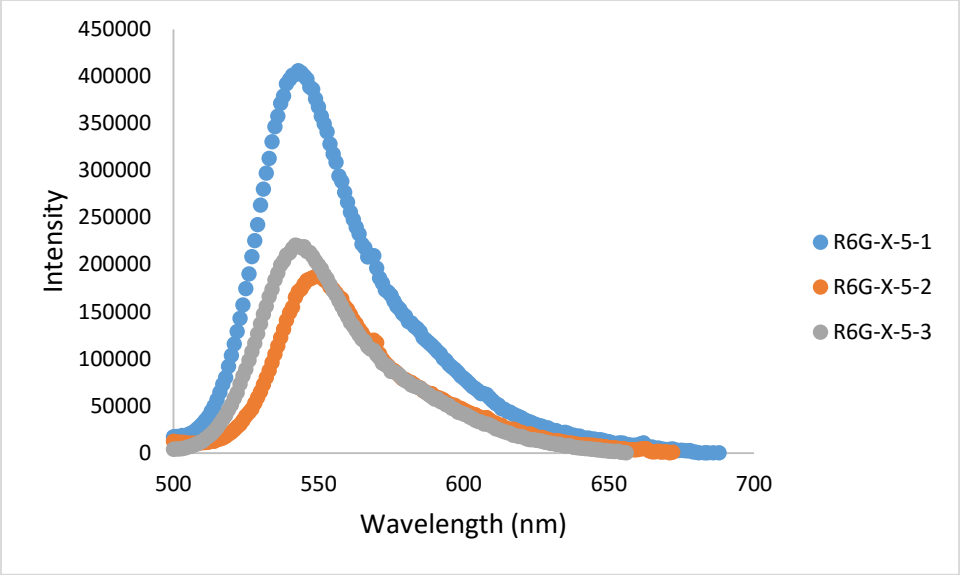

Figure 14: Emission spectra for three 10^{-6}-M R6G gel samples from batch R6G-X-5, excited at 465 nm, with 1-nm excitation and emission slit widths.

For Figure 14, the emission maxima ranged from 542 to 550 nm, and the maximum intensity ranged by just over a factor of two. Other samples exhibited a similar lack of homogeneity upon drying. In all cases, the lack of homogeneity of fluorescence intensity and maximum wavelength can be attributed to the samples decreasing in size by various amounts as they dried from wet gels to xerogels, resulting in variations in R6G concentration. From Figure 14 and other collected data, it appears the samples are mainly blue shifted from 550 nm.

R6G Aerogels

Aerogels were made with R6G concentrations of 10^{-4} and 10^{-6}-M. Not all the R6G aerogel monoliths appeared homogenous. In most aerogel batches the monoliths from the center four wells in each 16-well mold used experienced a significant amount of shrinkage. (Indeed, it is possible that for most batches using a 16-well mold, the center four monoliths were actually xerogels, rather than aerogels.) It appears that different wells in the mold undergo different

amounts of pressure and/or temperature in the hot press procedure. Currently it is unknown if this is caused by misaligned platens, a non-flat mold surface, another issue with mold design that gives rise to insufficient sealing of the center wells, or a combination of the aforementioned possibilities.

Rhodamine 6G aerogels also seemed to have non-homogenous maximum intensity and emission maxima, most likely due to this non-homogenous size and shape. Figure 15 displays the variation among fluorescence intensity and maximum wavelength for 10^{-4}-M R6G aerogels from the same batch.

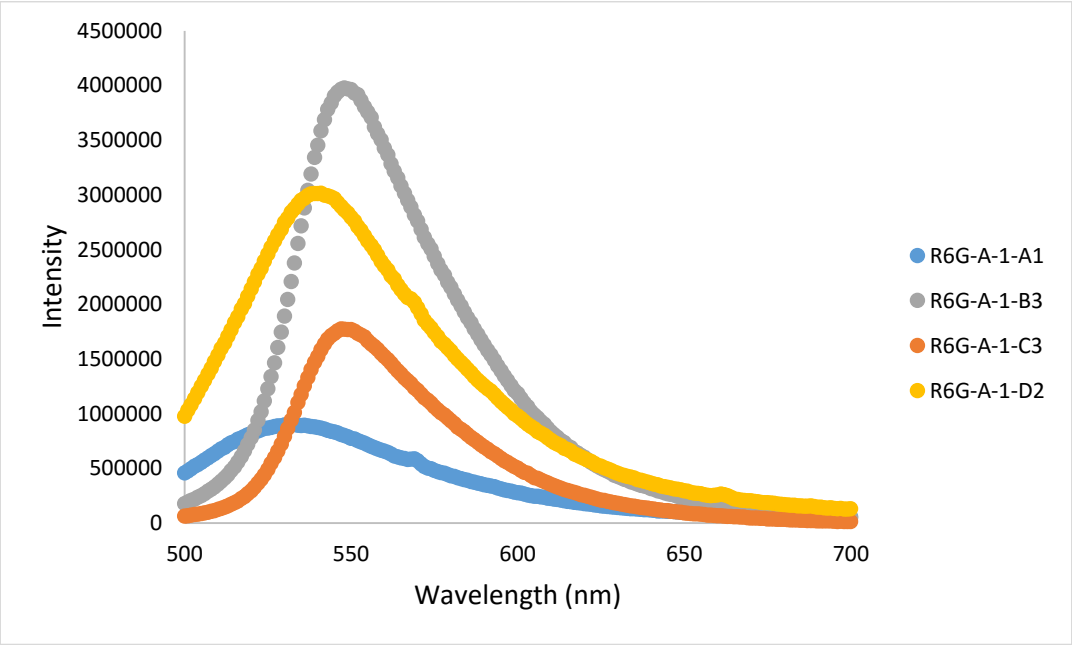

Figure 15: Overlaid emission spectra for 10^{-4}-M R6G aerogel samples from batch R6G-A-1, excited at 465 nm. Spectra for B3 and C3 had 1-nm excitation and emission slit widths, whereas spectra A1 and D2 had 2-nm excitation and emission slit widths.

Out of the batch of monoliths sampled for Figure 15, the center four monoliths experienced significant shrinkage, and were bright orange, while the outer-well monoliths

underwent little shrinkage, were opaque, and had the color of condensed cream. Figure 15 includes spectra of two of the center monoliths, B3 and C3, and two of the outer-well monoliths, A1 and D2. All four monoliths had different maximum wavelengths of fluorescence, ranging from 533 to 548 nm, and different peak emission intensities, varying by up to a factor of 4.42.

For the aerogels prepared with lower concentrations (10^{-6}-M), not all monoliths were observed to fluoresce. Figure 16 displays fluorescence spectra at different excitation wavelengths for a shrunken center monolith, whereas Figure 17 displays the fluorescence spectra at different excitation wavelengths for an outer-well monolith prepared in the same aerogel batch. Note that these outer-well monoliths did not exhibit fluorescence, whereas the shrunken center-well monoliths did. However, literature sources suggest that R6G is not sensitive to oxygen,[47] so even if fluorescence could become consistent among various R6G monoliths, it would not be a practical oxygen sensor probe by itself. It could potentially serve as a reference if incorporated into silica aerogels with a separate probe that was oxygen sensitive.

[47] A. Kahn, et al. "Fabrication of Oxygen-Sensor Films for Detecting and Treating Infections." *Interfaces and Surfaces NSF REU Site* (2013)

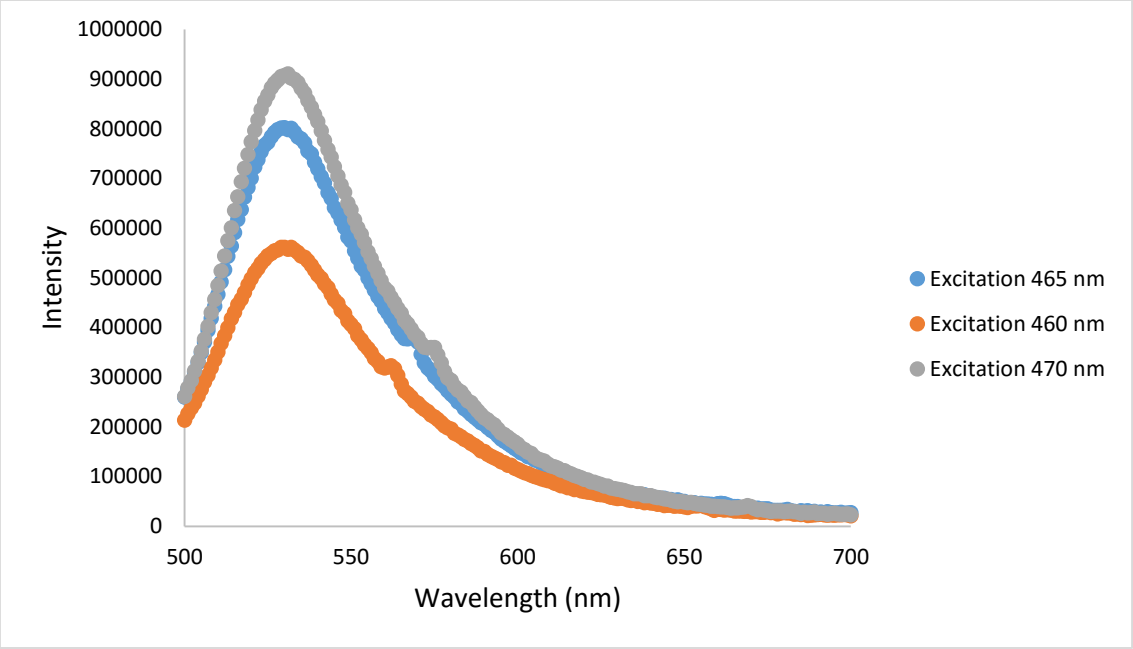

Figure 16: Overlaid emission spectra for 10^{-6}-M R6G inner-well aerogel sample, C3, from batch R6G-A-2, excited at the wavelengths specified in the legend, with 2-nm excitation and emission slit widths.

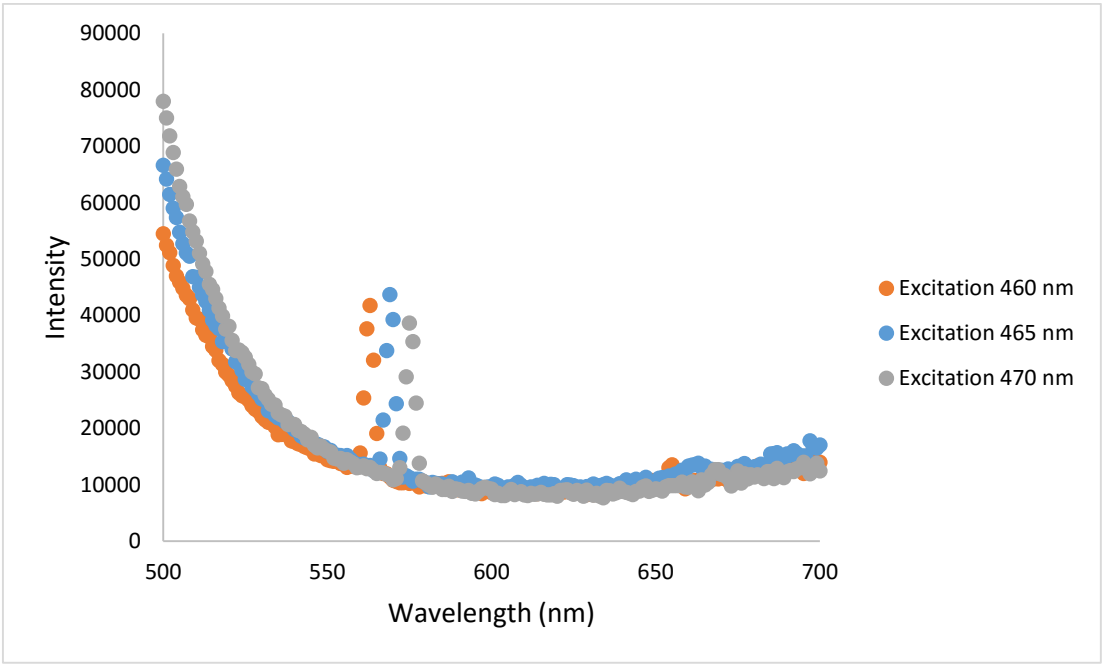

Figure 17: Overlaid emission spectra for 10^{-6}-M R6G outer-well aerogel sample, D1, from batch R6G-A-2, excited at various wavelengths, with 2-nm excitation and emission slit widths.

II. Platinum (II) Octaethylporphyrin

PtOEP Wet Gels & Xerogels

Upon excitation at 533 nm, all PtOEP wet gels had luminescence peaks centered at 643 nm. Spectra of most samples also had peaks around 610 and 651 nm. However, when the excitation wavelength was changed, the peak at 651 nm moved, indicating scatter. The emission spectra of a 10^{-5}-M PtOEP wet gel excited at different wavelengths is displayed in Figure 18.

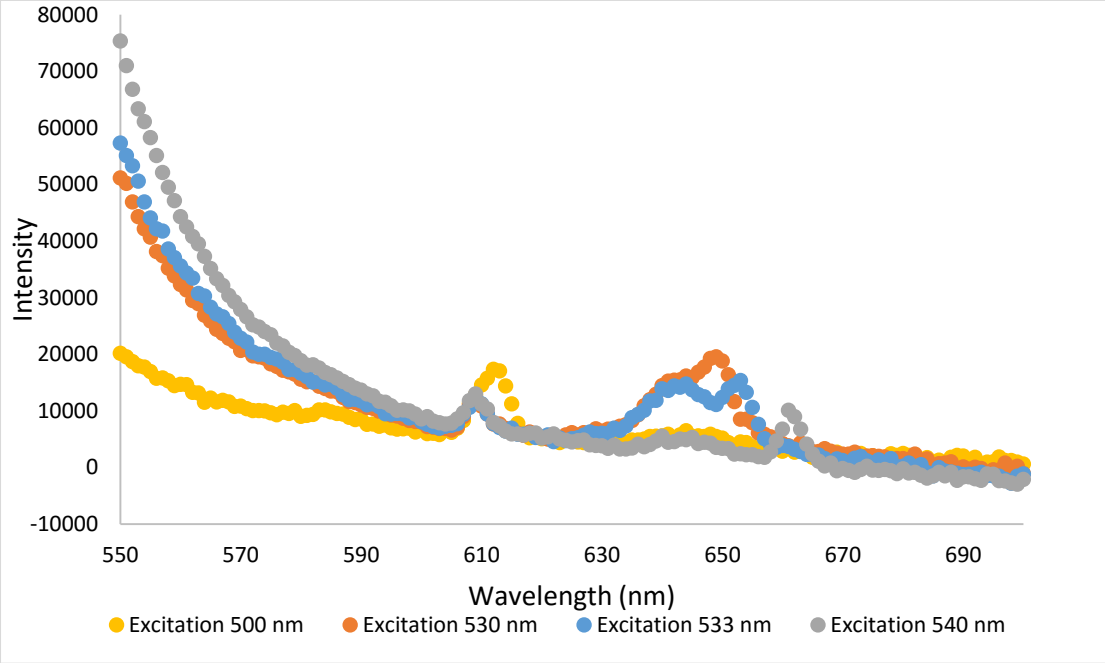

Figure 18: Overlaid emission spectra for 10^{-5}-M PtOEP wet gel sample, 1, from batch PtOEP-X-3, excited at various wavelengths, with 3-nm excitation and 2-nm emission slit widths. The peak at 609 nm for all excitation wavelengths except 500 nm is unknown. The scatter peak at 612 nm when the excitation wavelength is 500 nm seems to have disguised the unknown peak at 609 nm. The same scatter peak is observed at 649, 653 and 661 nm when the excitation wavelength is 530, 533, and 540 nm, respectively. The peak at 643 nm for each sample is due to luminescence.

As seen in Figure 18, the further the excitation wavelength varied from 533 nm, the more the scatter peak shifted away from the peak luminescence. However, changing the

excitation wavelength also caused the luminescence peak at 643 to weaken drastically in intensity. The peak at 609 nm did not seem to shift with changes in excitation wavelength. It seems the reason that a peak was not visible at 609 nm with 500 nm excitation, was due to the scatter peak at 612 nm masking it.

When the wet-gel samples dried into xerogels, the peak at 609 nm was hardly noticeable in the emission spectra. Unfortunately, the luminescence peak was also no longer noticeable. Exposing the xerogel monolith to 30 s of an N_2 purge did not reveal a noticeable change in luminescence.

A batch of 10^{-5}-M PtOEP wet gels was aged dried in three ways: (1) in capped cuvettes from which solvent vapor could not readily escape; (2) in uncapped cuvettes in a fume hood, which accelerated the drying process; (3) in parafilm-covered cuvettes with holes punched in the parafilm, for more gradual drying. The capped samples underwent little drying, with a single crack eventually running through the center of each monolith after four days. The uncapped samples were about a sixth of their initial size by the third day, with little internal cracking. By the fourth day, some were becoming cloudy and gaining multiple internal cracks. The parafilm-covered samples all dried uniquely, with various external edges shearing off by the third day, and uneven shrinking of samples by the fourth day. Emission spectra were taken daily and are shown in Figures 19-21.

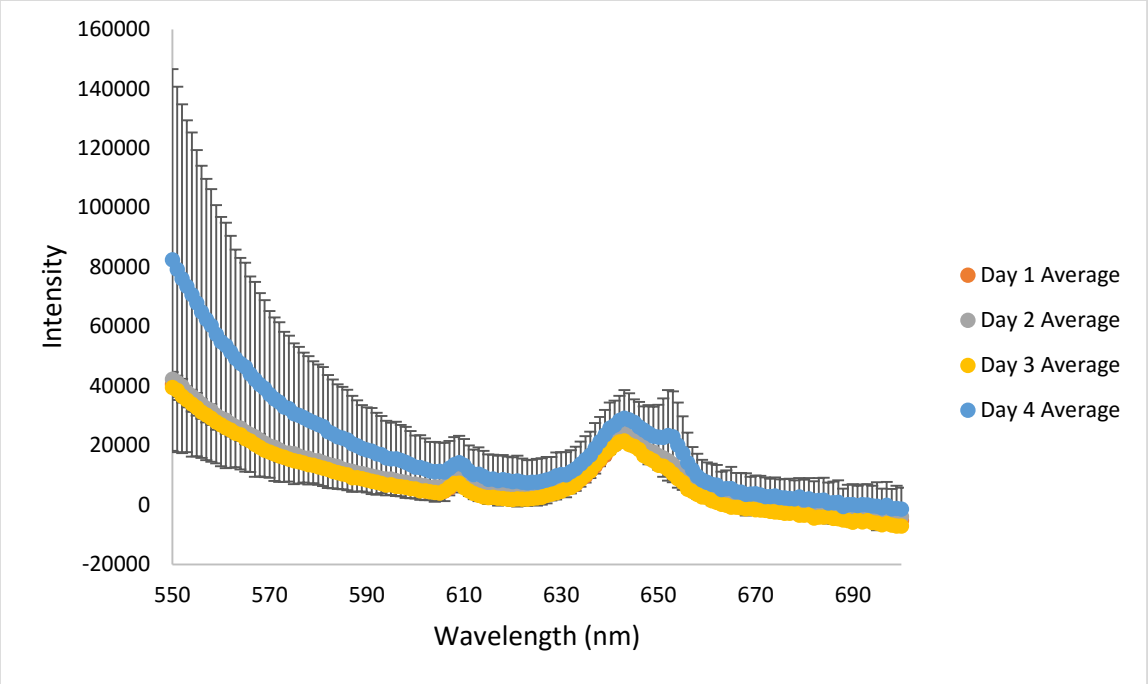

Figure 19: Overlaid emission spectra for aging of three PtOEP-X-5 capped wet gels over four days, where the excitation wavelength is 533 nm. Error bars indicate the variation among the three samples for each given day.

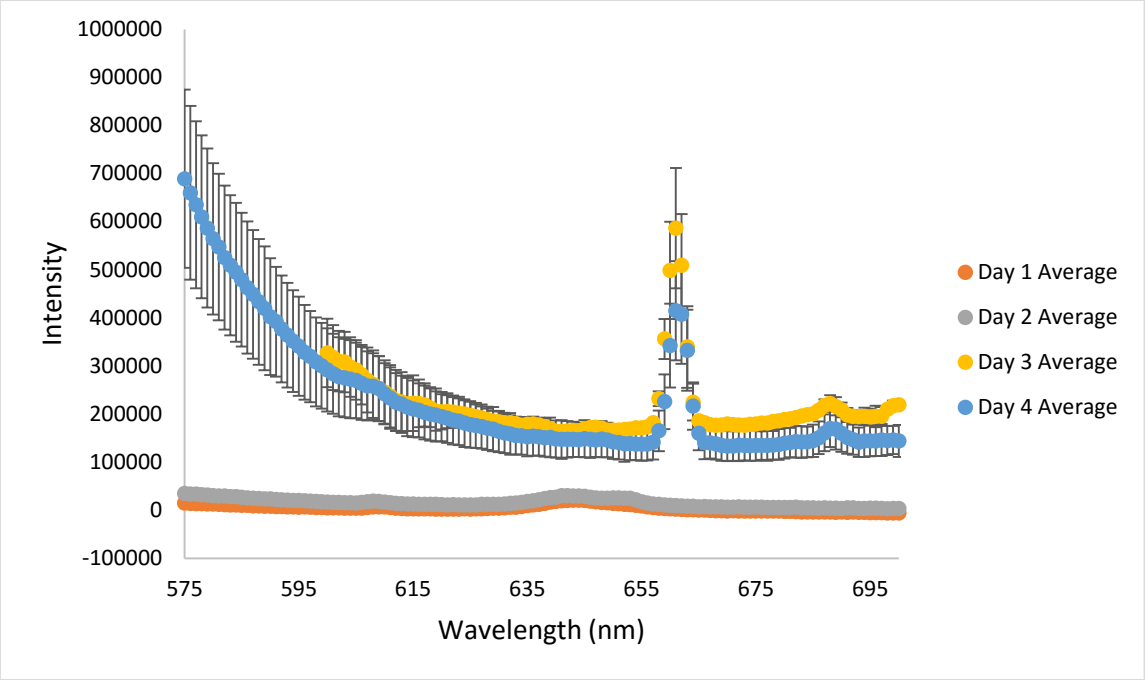

Figure 20: Overlaid emission spectra for aging of three PtOEP-X-5 uncapped wet gels over four days, where the excitation wavelength is 533 nm. Error bars indicate the variation among similar samples for each given day.

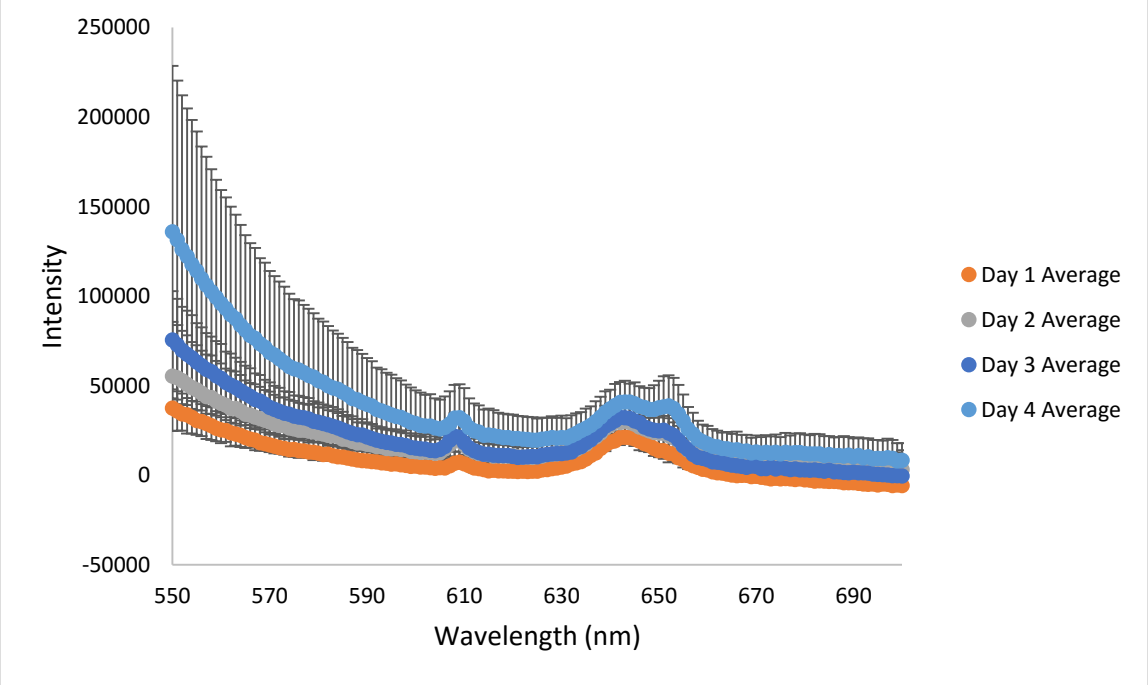

Figure 21: Overlaid emission spectra for aging of three PtOEP-X-5 broken parafilm-covered wetgels over four days, where the excitation wavelength is 533 nm. Error bars indicate the variation among similar samples for each given day.

From Figures 19-21, it appears that the luminescence was noticeable until the sample started drying. The capped and parafilm-covered samples (Figures 19 and 21, respectively) did not undergo a significant amount of drying over the course of four days, and retained their luminescence: a peak around 643 nm is visible in these spectra. By day 3, the uncapped sample (Figure 13) no longer exhibited the peak due to luminescence. At this point it was nearly fully dried to a xerogel, at about 1/6 the original volume. By day 4, there were internal cracks in the uncapped xerogel samples. As the samples shrunk, the intensity of background signal went up across all wavelengths, which could be a result of the uneven xerogel pieces scattering more light. However, the only peak still present above the background was the scatter peak around 660 nm.

The PtOEP moieties were assumed to be present inside the samples as they transitioned from wet gels to xerogels, as there was no evidence of precipitation in the gels. To determine whether the PtOEP moieties became immobilized within the gel in such a way as to be non-luminescent as the samples dried or whether enough O_2 was present in the dried sample to fully quench the PtOEP, an N_2 tank was hooked up directly to the cuvette.

Figure 22 shows emission at 643 nm as a function of time for a 10^{-5}-M PtOEP xerogel, as N_2 was cycled on and off.

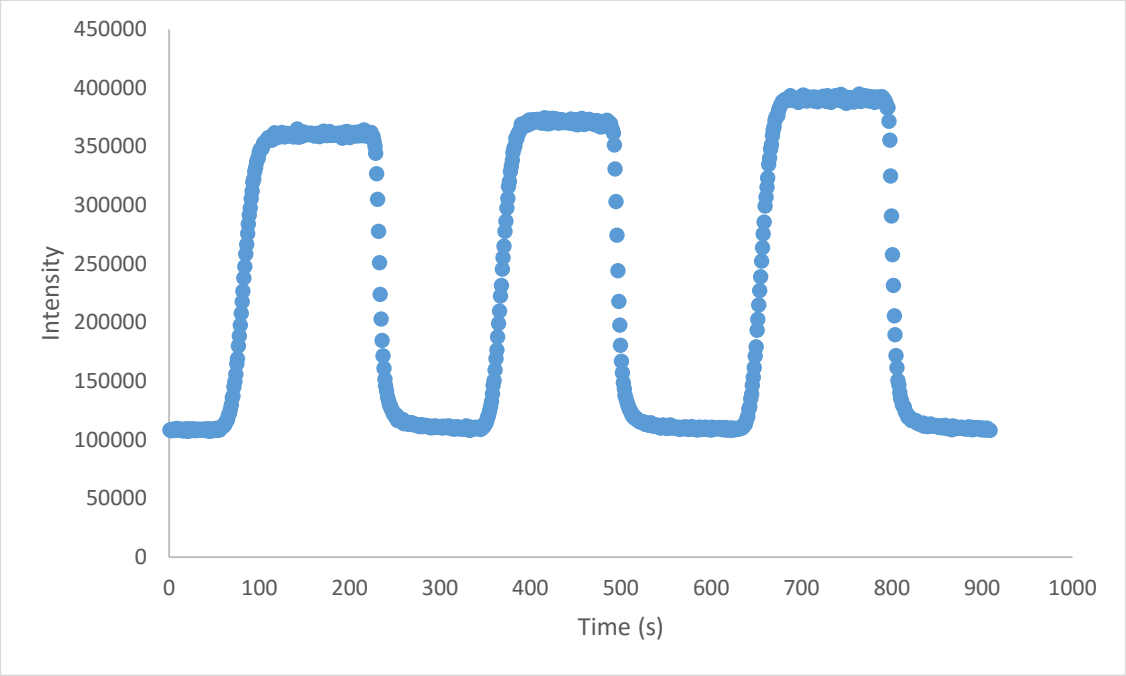

Figure 22: Time-based emission scan for 10^{-5}-M, PtOEP-X-5 sample 5 with N_2 cycling. Initially N_2 was off, and then switched on (ca. 60, 350, and 630 s) and off (ca. 220, 490, and 795 s). The excitation wavelength was 533 nm, emission wavelength was 643 nm, and there were 2-nm excitation and emission slit widths.

When N_2 was introduced into the cuvette, the luminescence intensity increased significantly within 30-40 s. This luminescence was reversible, and quickly returned to the intensity at ambient conditions within about 30-40 s after N_2 is shut off. Thus, the PtOEP-doped xerogels responded to O_2, as expected. When a 10^{-5}-M PtOEP xerogel was excited at 533 nm, the resulting overall signal was 3.52x higher at 646 nm when N_2 was flowing through the sample than the observed signal under ambient conditions (see Figure 23); however, there appeared to be no discernable emission peak at 646 nm under ambient conditions.

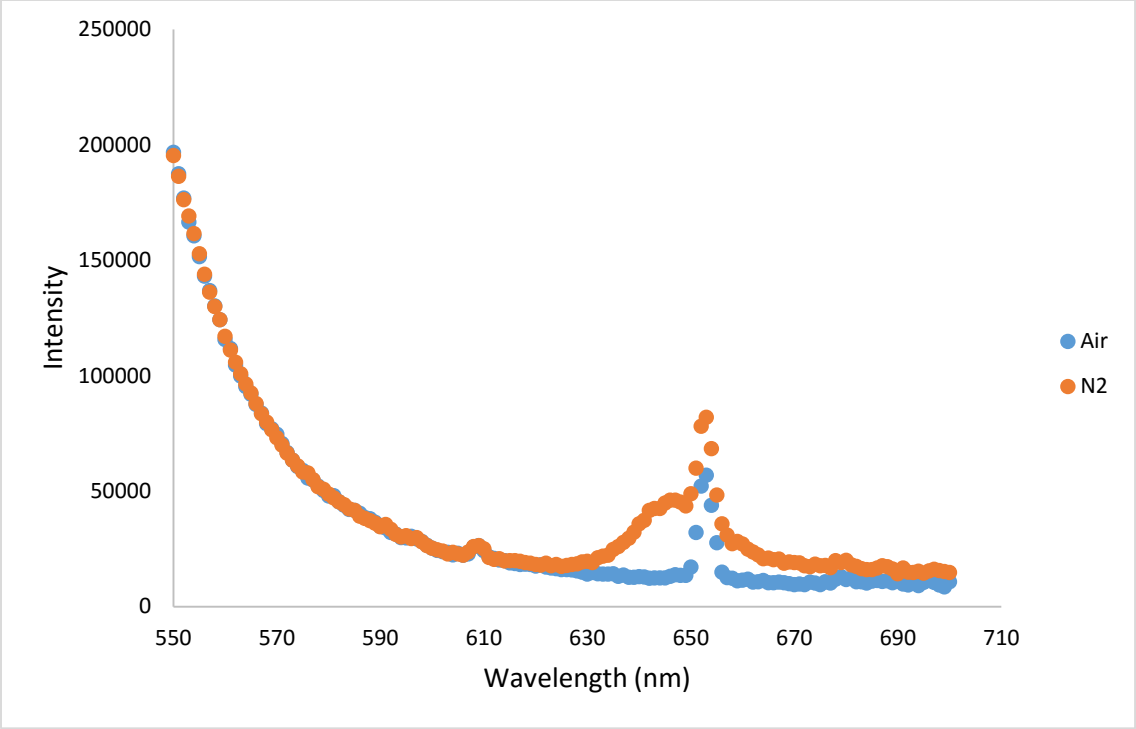

Figure 23: Overlaid emission spectra for 10^{-5}-M PtOEP xerogel sample, 5, from batch PtOEP-X-5 in an air and N_2 environment. Excited at 533 nm with 2-nm emission and excitation slit widths.

PtOEP Aerogels

As was the case for the R6G aerogels, all PtOEP aerogels fabricated in the 16-well mold exhibited larger, aerogel-like monoliths in the outer wells of the mold, and shrunken, xerogel-like monoliths in the inner wells. In an N_2 environment, monoliths from the center wells in the 16-well molds exhibited an increase in luminescence at 643 nm, as compared to ambient atmosphere. Figure 24 shows a time-based emission scan for a 10^{-5}-M PtOEP aerogel, with N_2 cycling.

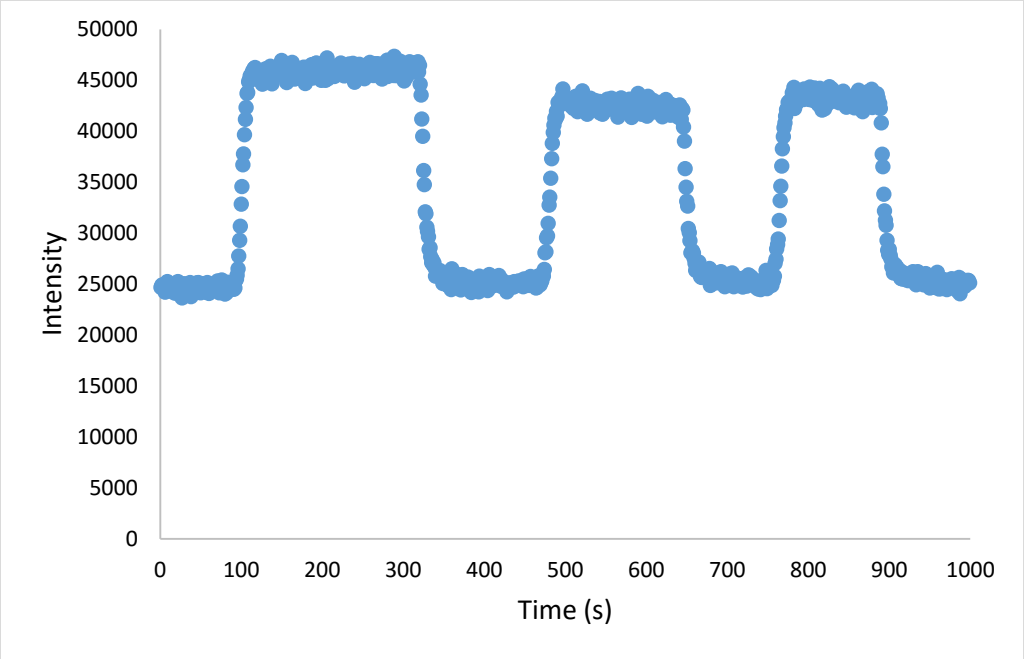

Figure 24: Time-based emission scan for 10^{-5}-M, PtOEP-A-2 sample B2, with N_2 cycling. Initially N_2 was off, and then switched on (ca. 90, 480, and 760 s) and off (ca. 320, 645, and 890 s). The excitation wavelength was 533 nm, emission wavelength was 643 nm, and there were 2-nm excitation and emission slit widths.

The sample was sensitive to O_2, with the luminescence intensity stabilizing within about 20 s after the addition or removal of O_2. The intensity was up to 1.9x higher in an oxygen-free environment than in air.

Center-well monoliths from batches with other concentrations of PtOEP aerogels also exhibited an increase in luminescence intensity in response to N_2. Figure 25 shows a time-based emission scan for an inner mold $3x10^{-5}$-M PtOEP aerogel, with N_2 cycling.

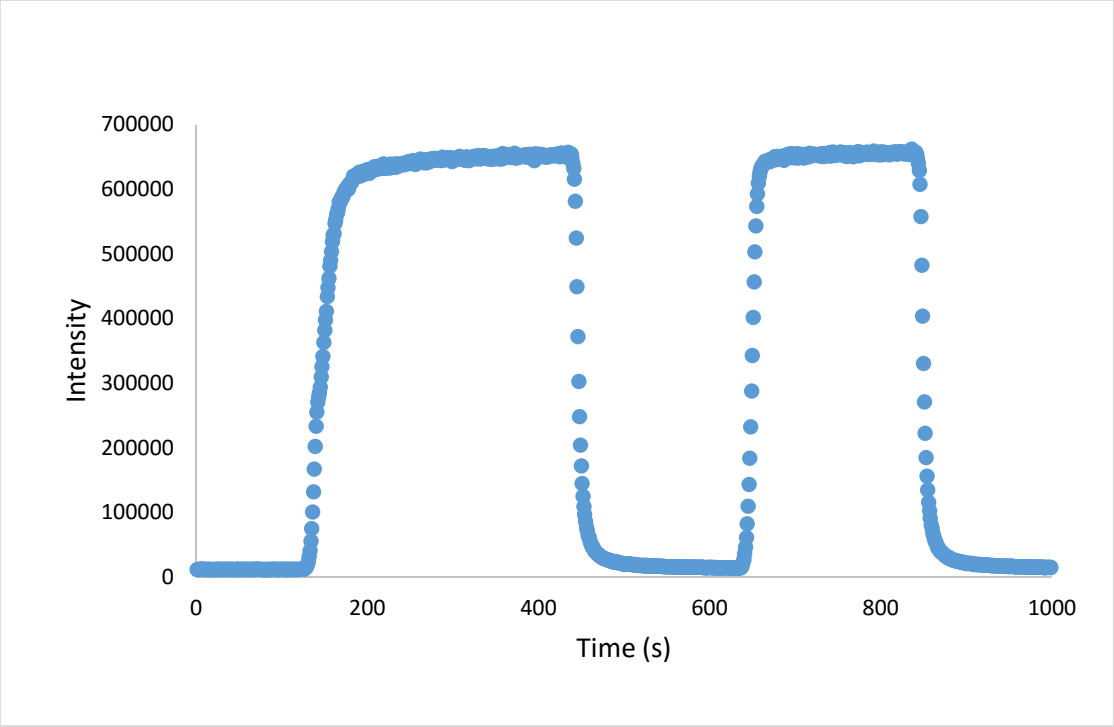

Figure 25: Time-based emission scan for $3x10^{-5}$-M monolith, PtOEP-A-4 sample B3, with N_2 cycling. Initially N_2 was off, and then switched on (ca. 126, and 636 s) and off (ca. 438, and 840 s). The excitation wavelength was 533 nm, emission scan was 643 nm, and there were 2-nm excitation and emission slit widths.

The sample was sensitive to O_2, with the luminescence intensity stabilizing within about 75 s after the removal of O_2, and within about 50 s after the addition of O_2. The intensity was up to 56x higher in an oxygen-free environment than in air.

Emission spectra for this monolithic sample in air and N_2 environments are shown in Figure 26. At the peak luminescent wavelength, 644 nm, the intensity was 257x higher in N_2 than in air. Normally a scatter peak appeared at 653 nm for the emission spectrum of PtOEP-doped samples excited at 533 nm under ambient conditions, as seen in Figure 26. However, the luminescence for the spectrum under N_2 had such a high intensity, that the scatter peak was not distinguishable under those conditions.

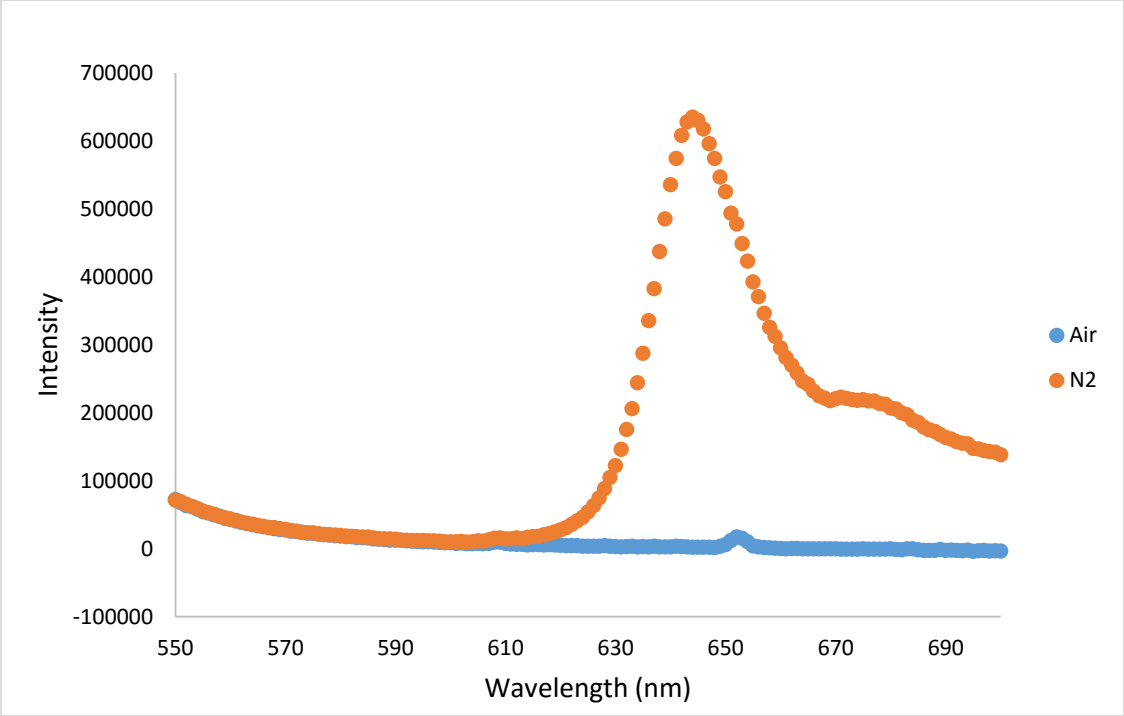

Figure 26: Overlaid emission spectra for $3x10^{-5}$-M, PtOEP-A-4 sample B2, in an air and N_2 environment. Excitation wavelength is 533 nm, and there are 2-nm excitation and emission slit widths.

The densities of some inner-well PtOEP monoliths are displayed in Table 13. The volume could not be assumed to be that of the mold, and thus was calculated from manually measured dimensions. Calipers were used to measure to the nearest 0.001 cm. Based on their densities, these monoliths appear to be more similar to xerogels than aerogels.

Table 13: Physical measurements of Inner-Well $3x10^{-5}$-M PtOEP-doped monoliths

batch-sample	mass (g)	volume (mL)	density (g/mL)
5-B3	0.1176	0.291	0.404
5-C2	0.1104	0.384	0.288
5-C3	0.1172	0.307	0.381
6-C3	0.1152	0.366	0.315
6-B3	0.1062	0.326	0.326

Outer-well monoliths, of both 10^{-5} and $3x10^{-5}$-M PtOEP concentration, did not appear to be sensitive to oxygen. Figure 27 displays a time-based emission scan for an outer-well $3x10^{-5}$-M PtOEP aerogel, with N_2 cycling. The sample did not have a large response to purging with N_2. While there was a small increase in intensity when N_2 was flowing through the cuvette, there was a low signal-to-noise ratio.

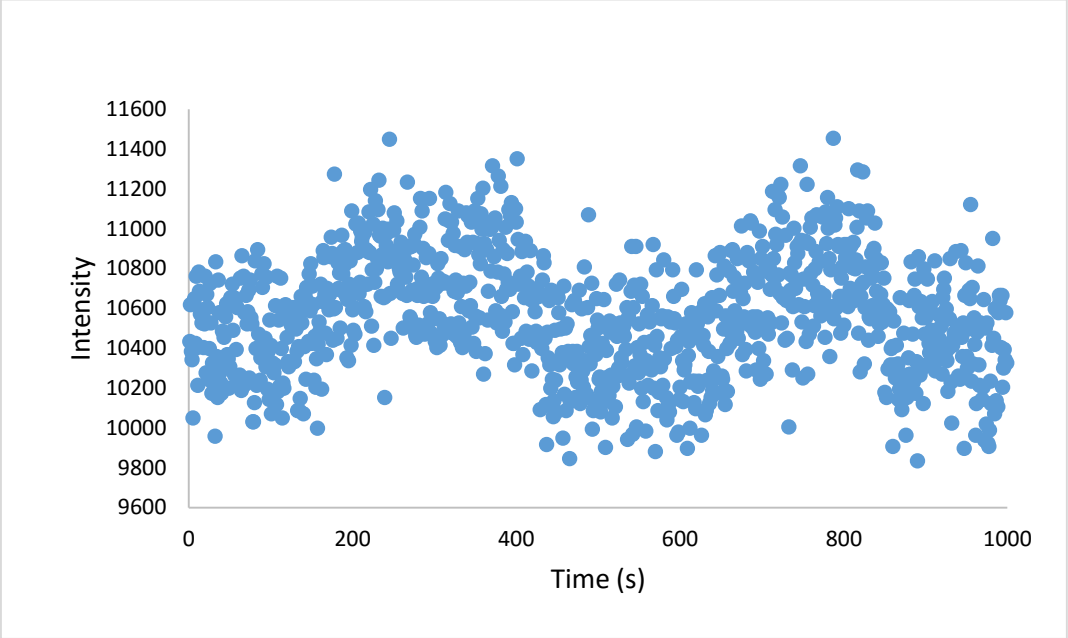

Figure 27: Time-based emission scan for $3x10^{-5}$-M, PtOEP-A-4 sample A4, with N_2 cycling. Initially N_2 was off, and then switched on (ca. 100, and 600 s) and off (ca. 400, and 840 s). The excitation wavelength was 533 nm, emission wavelength at 643 nm, and there were 2-nm excitation and emission slit widths.

Monoliths made with a hot press program using a higher restraining force (156 kN) and lower temperature (260 °C) were observed to be responsive to the removal of oxygen. Figure 28 shows a time-based emission scan for an outer-well $3x10^{-5}$-M PtOEP aerogel that had been manufactured under the adjusted hot press parameters. Figure 29 displays the emission spectra of this monolith, under air and N_2 conditions. The density measurements of some of these outer-

well monoliths made under the modified press parameters that are responsive to oxygen are displayed in Table 14.

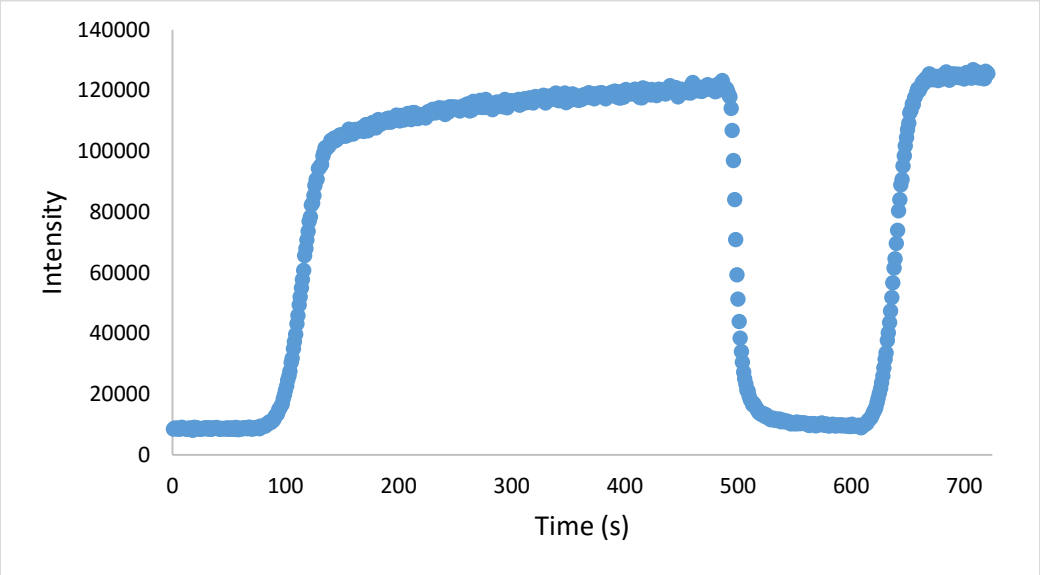

Figure 28: Time-based scan for $3x10^{-5}$-M, PtOEP-A-6 sample A4, with N_2 cycling. Initially N_2 was off, and then switched on (ca. 80, and 609 s) and off (ca. 489 s). The excitation wavelength was 533 nm, emission scan was at 643 nm, and there were 2-nm excitation and emission slit widths.

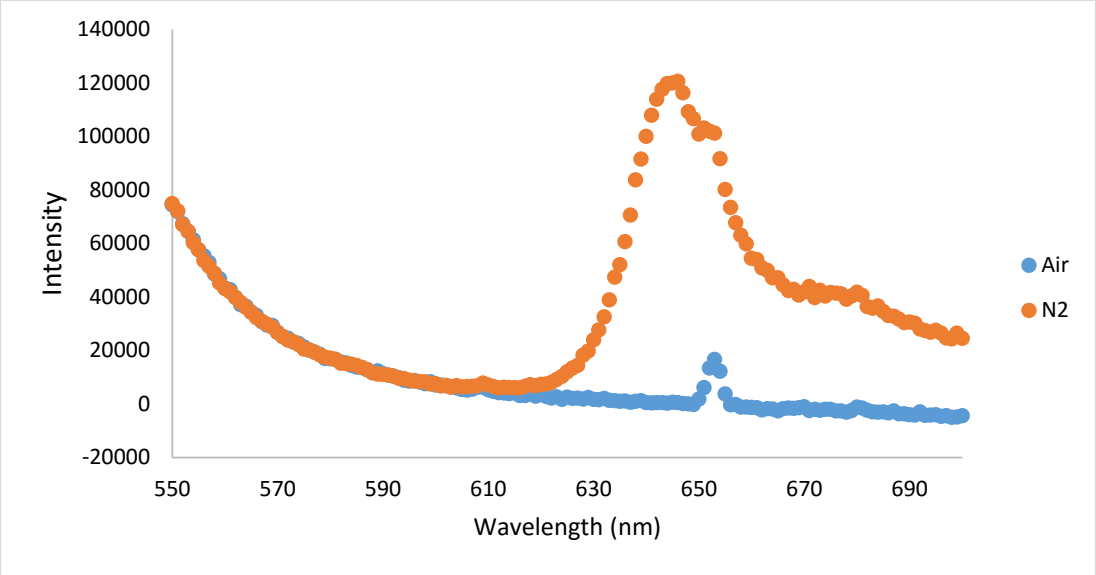

Figure 29: Overlaid emission spectra for $3x10^{-5}$-M, PtOEP-A-6 sample A4, in an air and N_2 environment. Excitation wavelength is 533 nm, and there are 2-nm excitation and emission slit widths.

Table 14: Physical measurements of Outer-Well $3x10^{-5}$-M PtOEP-doped aerogels			
batch-sample	**mass (g)**	**volume (mL)**	**density (g/mL)**
5-A1	0.124	1.27	0.0978
5-A3	0.0938	1.27	0.0738
5-B4	0.076	1.27	0.0599
5-D2	0.103	1.27	0.0812
5-D3	0.093	1.27	0.0732
6-A4	0.0996	1.27	0.0784
6-B4	0.128	1.27	0.101
6-D1	0.108	1.27	0.0847
6-D4	0.112	1.27	0.0886

Figure 28 displays the sensitivity to O_2 of the sample. The luminescence intensity stabilized within about 55 s after the removal of O_2 at 80 s. The monolith was reversibly sensitive to oxygen, and the ratio of an N_2 environment to air environment, I_{N2}/I_{air}, was up to 13.8. In

Figure 29, the intensity of the emission spectrum was significantly higher for luminescence in an N_2 environment than in air. At 646 nm, I_{N2}/I_{air} is 195.

Other outer-well monoliths from batches made using the modified processing conditions also responded to O_2. It appears that the temperature of the hot press procedure employed for the earlier data (Figures 24 to 27) was too high for the solutions in the outer wells, and that resulted in decomposition of the PtOEP moieties that were inside those molds, rendering the monoliths non-responsive. This is surprising, since work by a previous student demonstrated that aerogels fabricated using the 16-well cylindrical mold and hot-press parameters that reached 288 °C (550 °F) were responsive to the presence of O_2.[48] Table 15 displays the I_{N2}/I_{air} for various PtOEP monolith samples manufactured using the modified hot press parameters from Tables 7 and 8.

Table 15: PtOEP Aerogel Peak Luminescence Ratio with N_2

PtOEP Batch #	**Wavelength (nm)**	**I_{N2}/I_{air}**
Outer Well Monolith		
5 A1	644	461
5 D2	644	813
6 A4	646	195
6 D1	644	121
Inner Well Monolith		
4 B2	644	257
5 B3	645	20.9
6 C3	646	125

[48] A. F. Phillips, et al. "Fabrication and characterization of PtOEP-doped silica aerogels for use as oxygen sensors." (2006)

A series of time-based emission scans were performed on the luminescent PtOEP aerogel samples (both inner and outer-well monoliths, $3x10^{-5}$-M PtOEP, from batch PtOEP-A-6) fabricated using the modified lower-temperature hot-press procedure, replacing a bottle of N_2 with a bottle of mixed gas. This bottle was a combination of 5.025 mol% O_2 and 94.975 mol% N_2. These tests were done to see how responsive the samples were to low levels of O_2, since at ambient conditions they were fully quenched.

Like all prior time-based emission scans, these were performed starting at ambient conditions. Instead of turning on an N_2 tank displacing the air in the cuvettes, the mixed gas tank was turned on, filling the cuvettes with 5% O_2. For both outer and inner-well samples, there was no discernable luminescence in the 5% O_2 environment, similar to when they were under ambient conditions. Taking emission spectra at 533 nm for these samples in both ambient conditions and the 5% O_2 conditions yielded no luminescence, with the only noticeable signal being the scatter peak around 653 nm. Thus, it appears that with only 5% O_2, PtOEP is still fully quenched.

A series of time-based emission scans were performed using a gas proportioner, an N_2 tank, and either the 5% O_2 blend gas, or a 0.53% O_2 blend gas tank. With these tanks and the gas proportioner, the luminescence of samples could be measured at 0.06, 0.12, 0.22, 0.31, 0.41, 0.53, 0.6, 1.2, 2.1, 2.9, 3.8, and 5.0% O_2, along with 0% and ~21% (for pure N_2, and ambient conditions, respectively). Multiple time-based emission scans were performed on an inner-well sample (PtOEP-A-6 C3), an outer-well sample (PtOEP-A-5 A1), and a fragment from the large monolith for optical testing (PtOEP-A-7).

Figure 30 is a time-based emission scan for which a gas proportioner was used to vary the concentration of O_2 flowing through the sample. The O_2 concentration ranged from 0% in full

N_2 environment, to about 21% in air, with measurements taken at oxygen concentrations of about 0, 1, 2, 3, 4 and 5%.

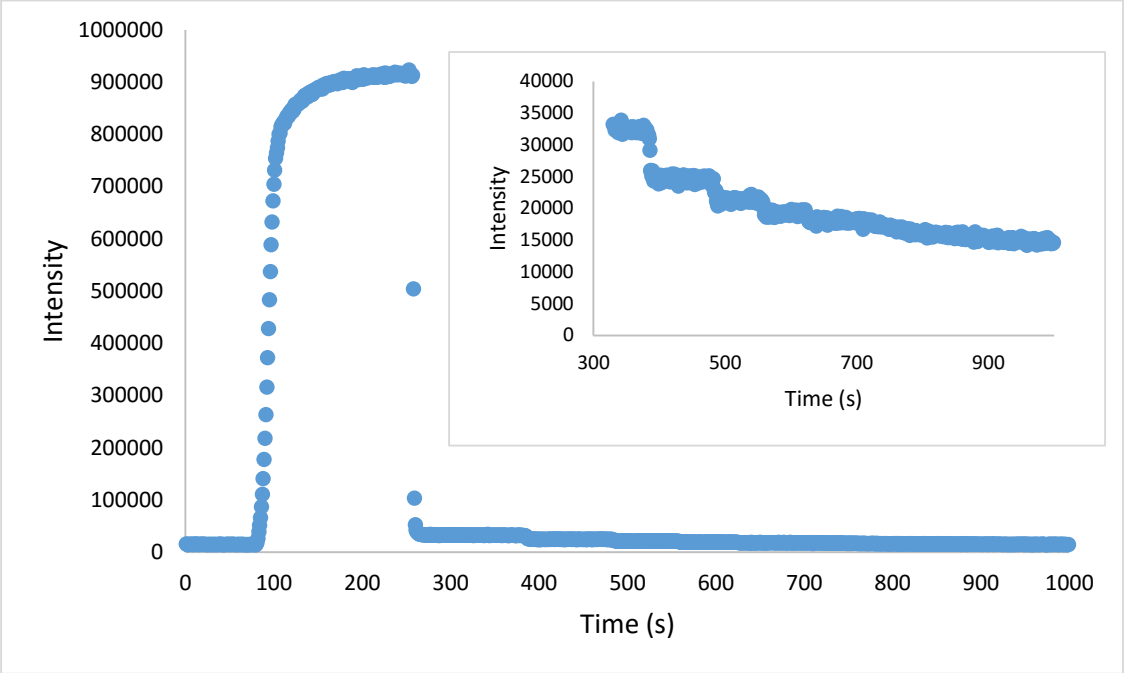

Figure 30: Time-based emission scan for $3x10^{-5}$-M PtOEP monolith, sample C3 from batch PtOEP-A-6 with varying O_2 concentration. The scan starts in ambient conditions. At 80, 250, 360, 480, 555, 620, and 690 s, the mixture of gas was changed so that there would be 0, 1.2, 2.1, 2.9, 3.8, 5.0, and 21% O_2, respectively The excitation wavelength was 533 nm, emission scan was at 643 nm, and there were 2-nm excitation and emission slit widths. Inset is the portion of the emission scan from 330 s onward.

The initial change in intensity in Figure 30 is similar to that for other time-based emission spectra when the environment is switched from air to N_2, with a rapid initial increase in intensity. For each variation of O_2%, it took the sample about 15 s for the luminescence to stabilize.

The luminescence of PtOEP is shown to be responsive to O_2 concentration and consistently decrease as the concentration of O_2 increases. From Figure 30, it only took roughly 1% O_2 in the gas blend to bring the intensity down by a factor of 25.8. While Figure 30 is just for

an inner-well monolith (PtOEP-A-6, sample C3), the outer-well monolith, and large monolith fragment both yielded similar time-based emission scans at this oxygen range.

Figure 31 is a time-based emission scan for which a gas proportioner was used to vary the concentration of O_2 flowing through the sample. The O_2 concentration ranged from 0% in full N_2 environment, to about 21% in air, with measurements taken at about 0, 0.06, 0.12, 0.22, 0.31, 0.41, 0.53% O_2 concentrations.

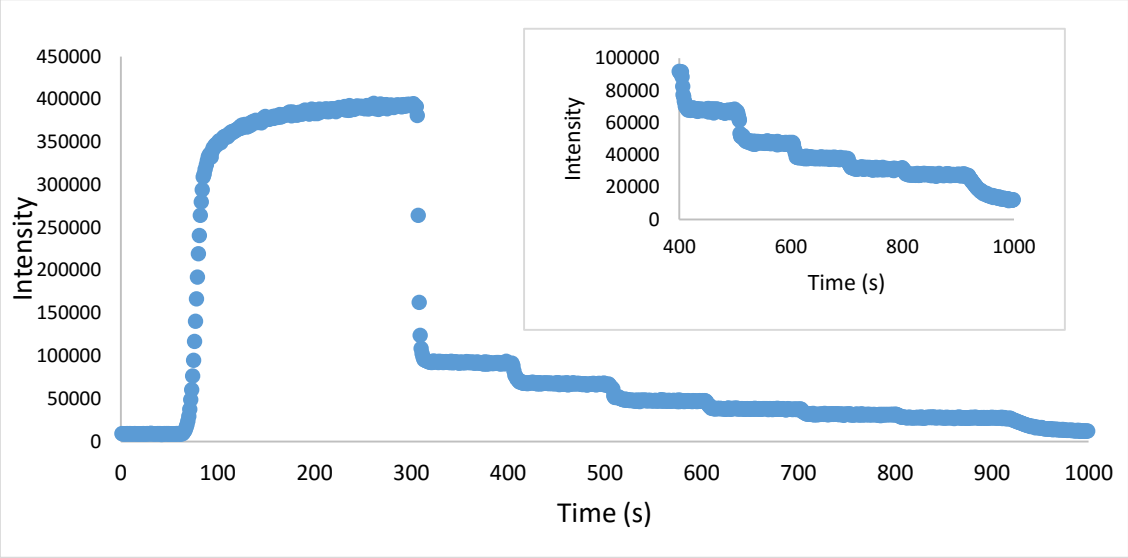

Figure 31: Time-based emission scan for $3x10^{-5}$-M PtOEP monolith, sample C3 from batch PtOEP-A-6 with varying O_2 concentration. The scan starts in ambient conditions. At 60, 300, 400, 500, 600, 700, and 800 s, the mixture of gas was changed so that there would be 0, 0.06, 0.12, 0.22, 0.31, 0.42, 0.53, and 21% O_2, respectively The excitation wavelength was 533 nm, emission scan was at 643 nm, and there were 2-nm excitation and emission slit widths. Inset is the portion of the emission scan from 330 s onward.

The luminescence of PtOEP was shown to be responsive to O_2 concentration and consistently decreased as the concentration of O_2 increases. As can be seen in Figure 31, it took roughly 0.06% O_2 in the gas blend to bring the intensity down by a factor of 4.1. While Figure 31

is just for an inner-well monolith (PtOEP-A-6, sample C3), the outer-well monolith, and large monolith fragment both yielded similar time-based emission scans at this oxygen range.

For all samples, repeat measurements over a period of weeks determined that time since fabrication had no significant effect on the luminescence of PtOEP-doped aerogels in the presence of oxygen. Figures 32, 33, and 34 are the Stern-Volmer plot for an inner-well monolith, an outer-well monolith, and the large monolith fragment. Values for each plot were calculated by averaging all of the time-based emission scans performed on those samples.

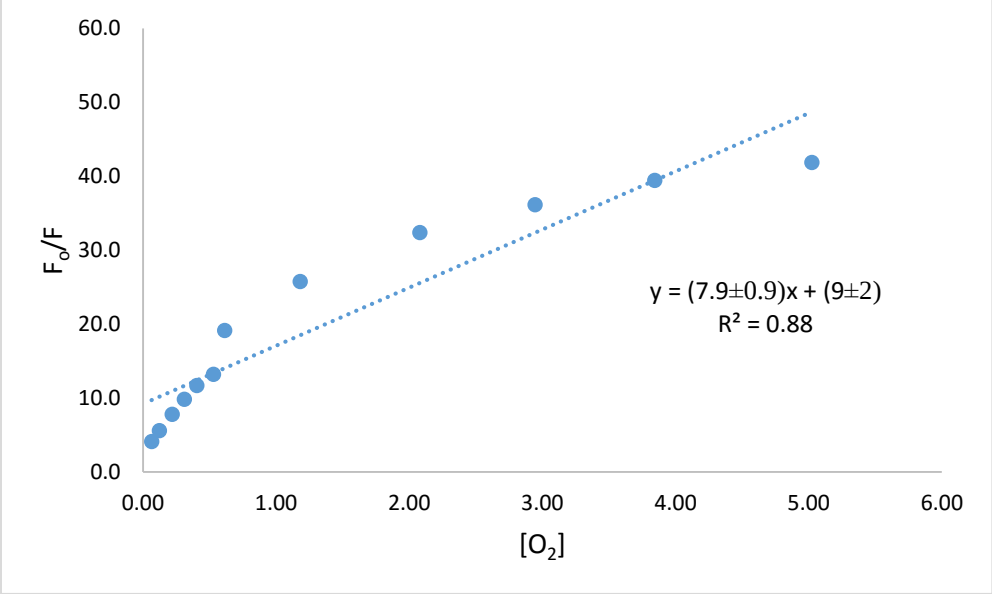

Figure 32: Stern-Volmer plot for $3x10^{-5}$-M PtOEP monolith, sample C3 from batch PtOEP-A-6, with LINEST function. All data points are an average of the ratio of unquenched to quenched luminescence for each concentration of oxygen determined from the time-based emission scans.

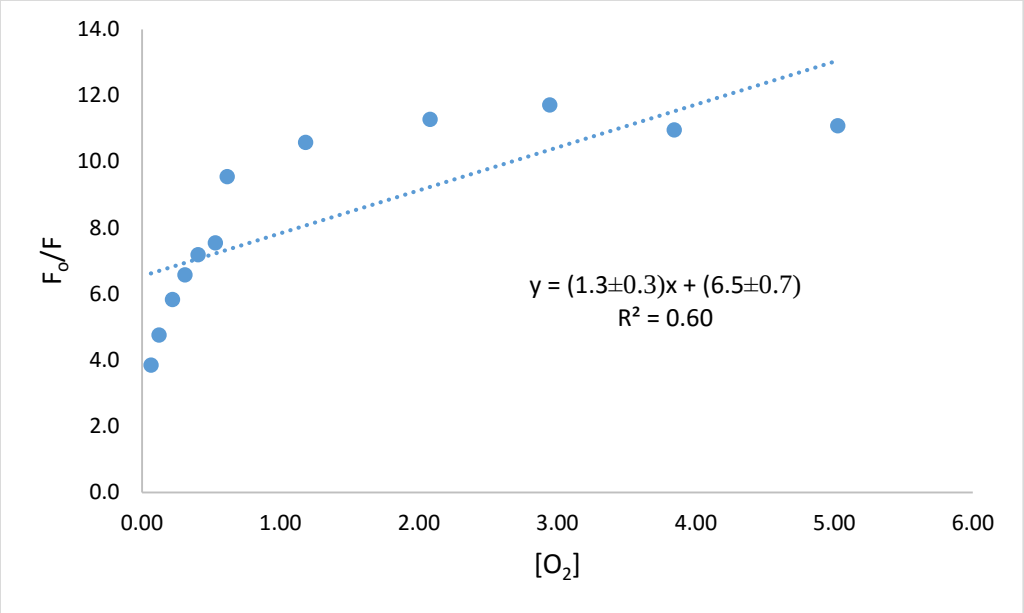

Figure 33: Stern-Volmer plot for 3x10^{-5}-M PtOEP monolith, sample A1 from batch PtOEP-A-5, with LINEST function. All data points are an average of the ratio of unquenched to quenched luminescence for each concentration of oxygen determined from the time-based emission scans.

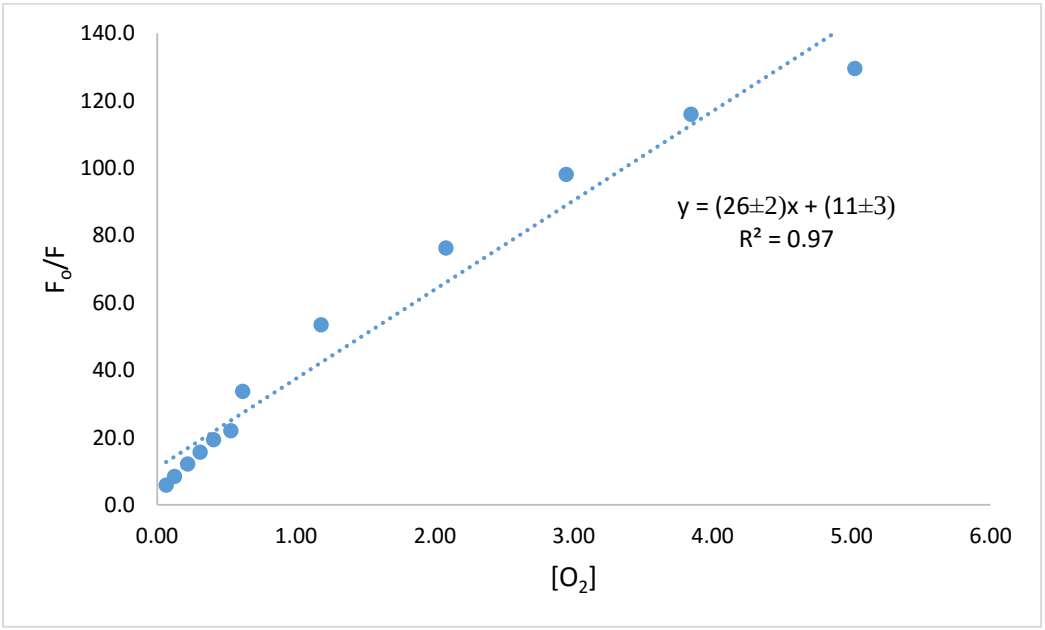

Figure 34: Stern-Volmer plot for 3x10^{-5}-M PtOEP monolith, fragment from batch PtOEP-A-7, with LINEST function. All data points are an average of the ratio of unquenched to quenched luminescence for each concentration of oxygen determined from the time-based emission scans.

The Stern-Volmer plots in Figures 32-34 are clearly not linear. Thus, the PtOEP probes in the silica aerogels are not all located in the same type of accessible microenvironment. A modified Stern-Volmer equation was used (equation 2) to try to model what is happening inside the samples. This equation assumes that a portion of the PtOEP probes inside the silica aerogels is inaccessible to the quencher, oxygen. For the modified Stern-Volmer equation, the ratio of the unquenched luminescence to the difference of the unquenched and quenched luminescence is plotted against the inverse of the concentration of quencher. The inverse of the y-intercept is the fractional amount of accessible probe. Figures 35, 36, and 37 are the modified Stern-Volmer plots for an inner-well monolith, an outer-well monolith, and the large monolith fragment. The fractional accessibility and K_{sv} of the microenvironment of the various samples determined from Figures 35 through 37, along with the R^2 for those respective figures are compiled in Table 16.

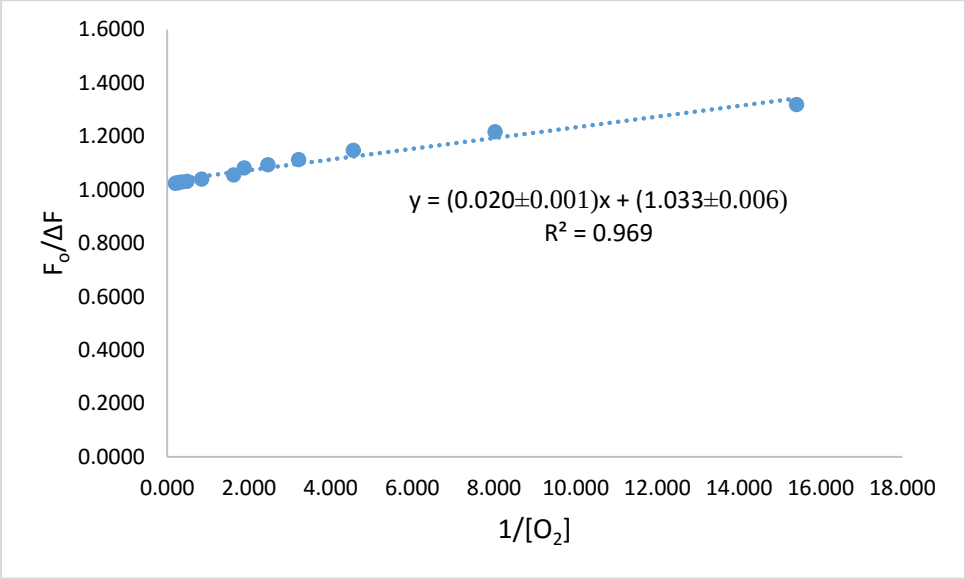

Figure 35: Modified Stern-Volmer plot for $3x10^{-5}$-M PtOEP monolith, sample C3 from batch PtOEP-A-6, with LINEST function. All data points are an average of the ratio of unquenched to the difference of unquenched and quenched luminescence for each concentration of oxygen determined from the time-based emission scans.

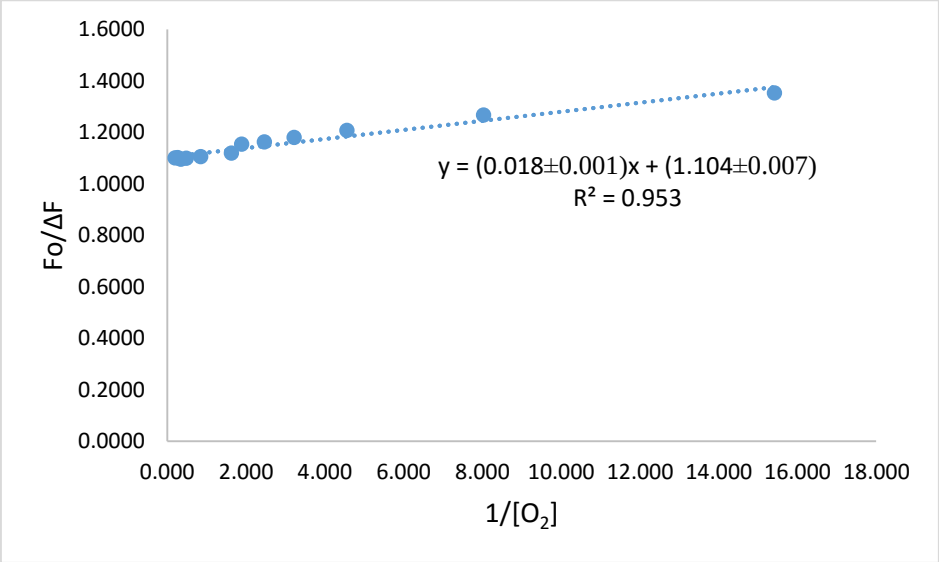

Figure 36: Modified Stern-Volmer plot for $3x10^{-5}$-M PtOEP monolith, sample A1 from batch PtOEP-A-5, with LINEST function. All data points are an average of the ratio of unquenched to the difference of unquenched and quenched luminescence for each concentration of oxygen determined from the time-based emission scans.

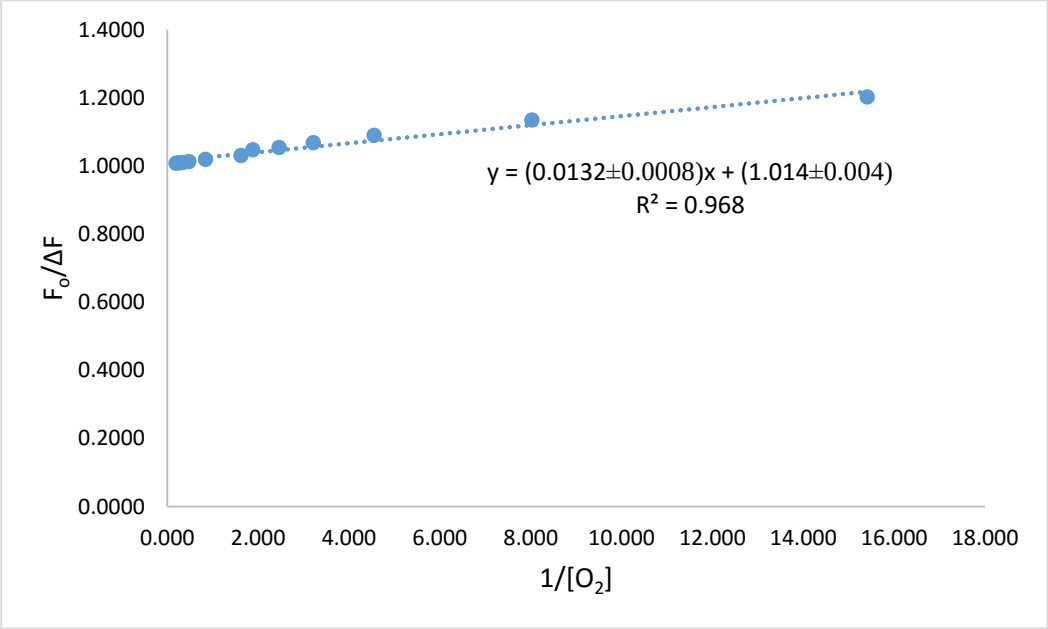

Figure 37: Modified Stern-Volmer plot for $3x10^{-5}$-M PtOEP monolith, fragment from batch PtOEP-A-7, with LINEST function. All data points are an average of the ratio of unquenched to the difference of unquenched and quenched luminescence for each concentration of oxygen determined from the time-based emission scans.

Table 16: Fractional accessibility, K_{sv}, and R^2 values for various PtOEP-doped samples for one-site accessible model (Modified S.V.)			
	PtOEP-A-6 C3	PtOEP-A-5 A1	PtOEP-A-7 fragment
f_1	0.9683	0.9055	0.9864
K_{sv1}	51	63	76.5
R^2	0.969	0.953	0.968

The best-fit lines in Figures 35-37 have R^2 values >0.95, so it appears that the modified Stern-Volmer equation was a reasonably good model for the incorporation of PtOEP probes in silica aerogels. According to these fits, approximately 97% of the PtOEP in the center-well monolith, 90% of the PtOEP in the outer-well monolith, and 99% of the PtOEP in the fragment from the large monolith was accessible to oxygen.

A two-microenvironment model was applied to the Stern-Volmer plots for an inner-well monolith, an outer-well monolith, and a fragment from the large monolith used in the proof-of-concept rig. These models used KaleidaGraph and fitted equation 3 to the Stern-Volmer plots. Figures 38-40 show fits of these two-microenvironment models to data obtained for the inner-well monolith, the outer-well monolith, and the large monolith fragment, respectively.

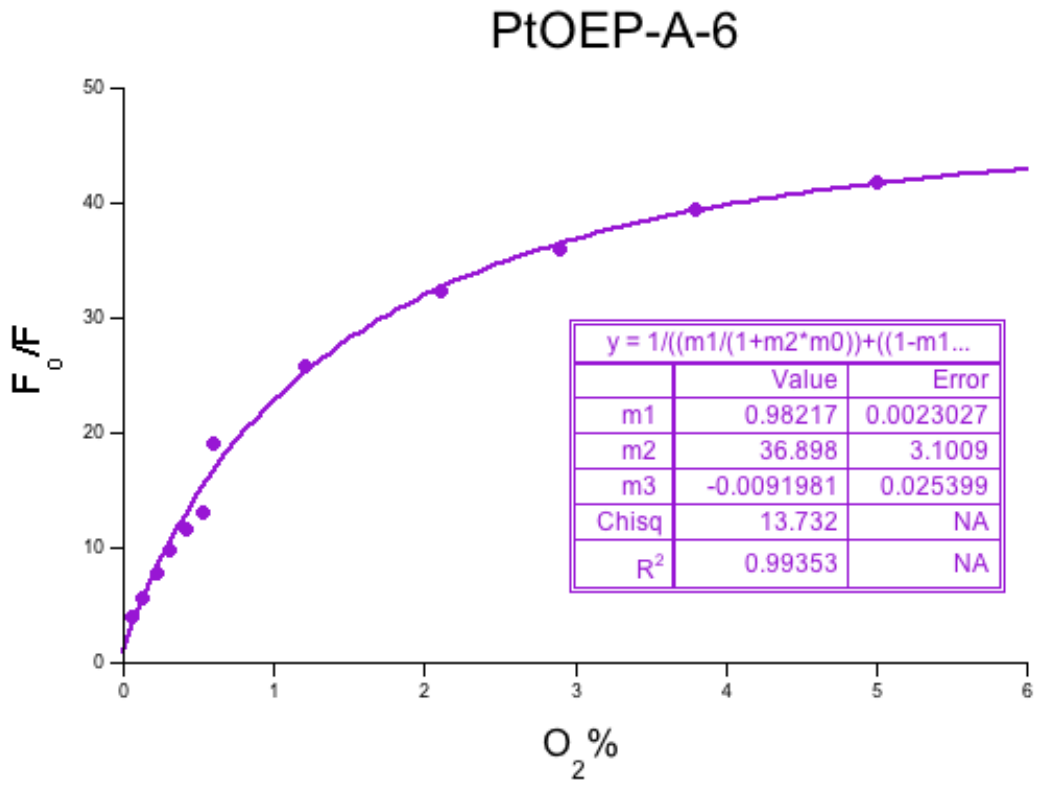

Figure 38: Two-site model for Stern-Volmer plot of $3x10^{-5}$-M PtOEP monolith, sample C3 from batch PtOEP-A-6, using KaleidaGraph. All data points are an average of the ratio of unquenched to quenched luminescence for each concentration of oxygen determined from the time-based emission scans.

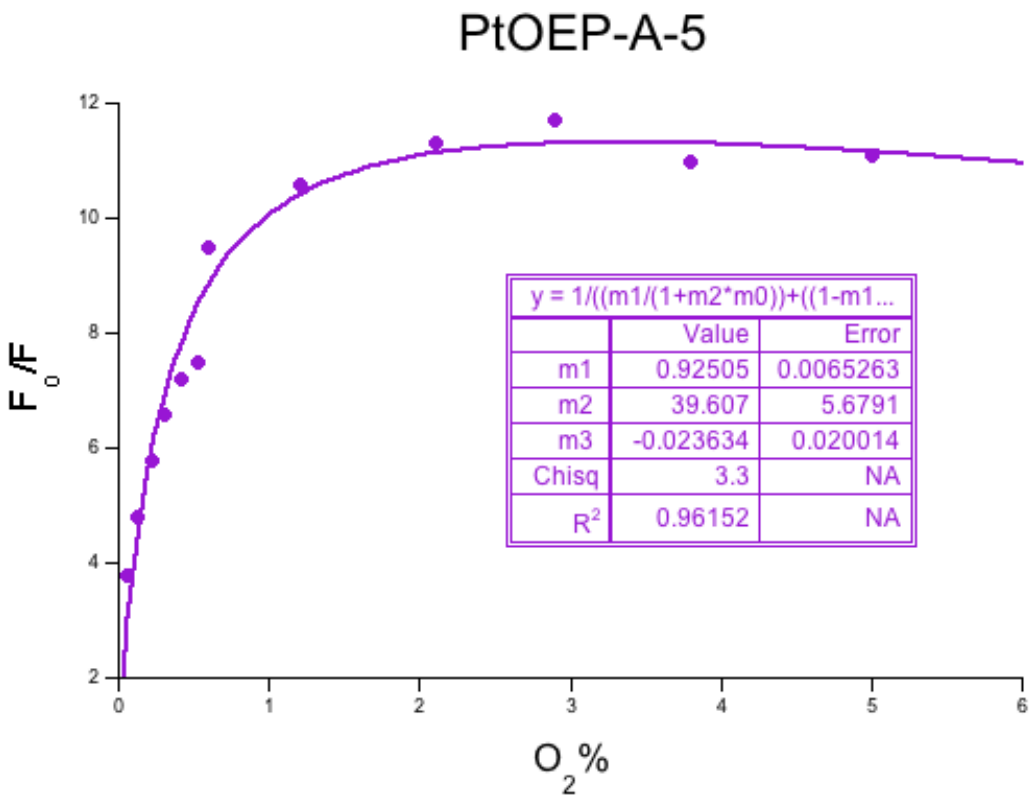

Figure 39: Two-site model for Stern-Volmer plot of $3x10^{-5}$-M PtOEP monolith, sample A1 from batch PtOEP-A-5 using KaleidaGraph. All data points are an average of the ratio of unquenched to quenched luminescence for each concentration of oxygen determined from the time-based emission scans.

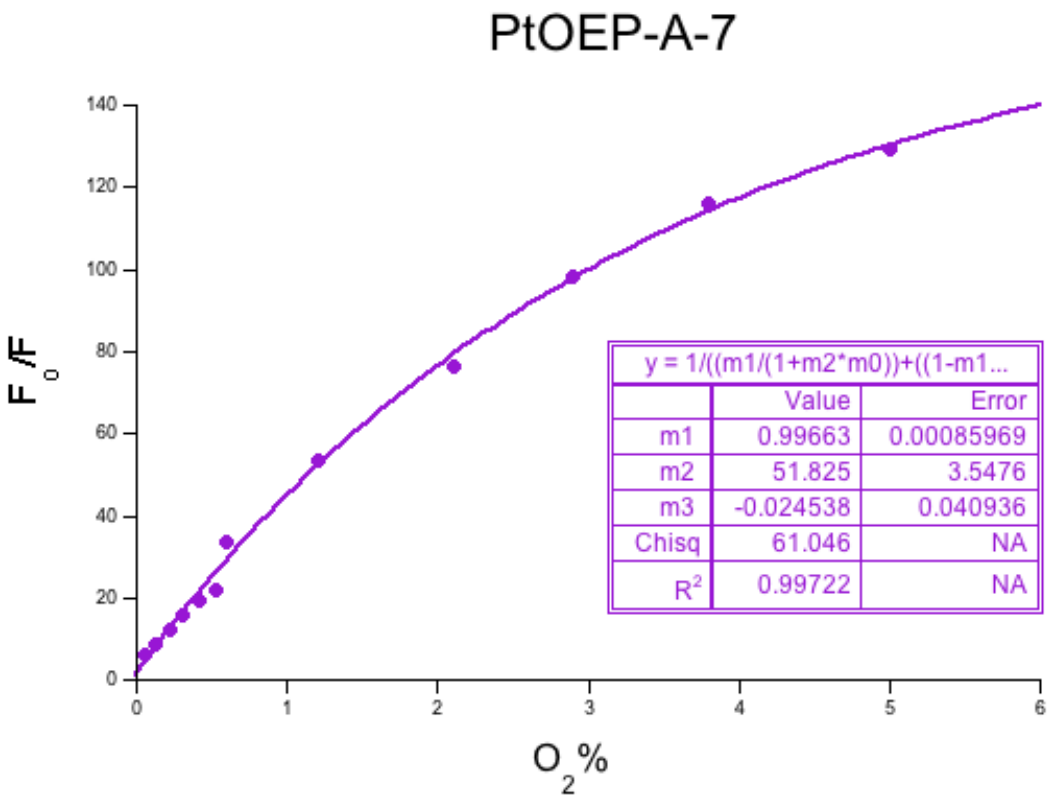

Figure 40: Two-site model for Stern-Volmer plot of $3x10^{-5}$-M PtOEP monolith, fragment from batch PtOEP-A-7, using Kaleidagraph. All data points are an average of the ratio of unquenched to quenched luminescence for each concentration of oxygen determined from the time-based emission scans.

The fractional accessibility of the main microenvironment in each sample is displayed in Table 17, along with the Stern-Volmer constant for both microenvironments and the R^2 values for the related figures. Note that since it is a two-site model, the fractional accessibility of the lesser accessible site is simply $1 - f_1$.

Table 17: Fractional accessibility, K_{sv}, and R^2 values for various PtOEP-doped samples for two-site accessible model (KaleidaGraph)			
	PtOEP-A-6 C3	PtOEP-A-5 A1	PtOEP-A-7 fragment
f_1	0.982±0.002	0.925±0.006	0.9966±0.0009
K_{sv1}	37±3	40±6	52±4
K_{sv2}	-0.01±0.02	-0.02±0.02	-0.02±0.04
R^2	0.994	0.961	0.997

The fractional accessibility for the main microenvironment of each sample for the two-site model is similar to that from the modified-Stern Volmer equation for the only accessible microenvironment. Comparing Table 17 to Table 16, it appears that for each sample, the two-site model has a fractional accessibility about 0.015 to 0.02 higher than what the one-site model predicted. However, the R^2 values for the two-site models all range between 0.961 and 0.997, where the one site model had R^2 values that ranged between 0.953 and 0.969. Due to the higher R^2 values, it can be assumed that the two-site model is a more accurate fit of the probe accessibility in the samples.

For the two-site model, none of the samples have an f_1 to be 1 within error. Based off the f_1 values, and the fact that f_2 is $1 - f_1$, there should be some accessibility in the second microenvironment, albeit a miniscule amount. However, upon observing the K_{sv2} values from Table 17, they are all 0, within error. A K_{sv} of 0 means that there is no accessibility in that microenvironment. Thus the two-site model and the one-site model seem to predict the same thing: that there is one microenvironment the probe is located in that is accessible to the quencher, and one that is inaccessible.

It has been proven that PtOEP-doped aerogels are responsive to oxygen content. That luminescence reversibly changes intensity based on concentration of oxygen, and responds

quickly to changes in oxygen content. However, from the varying concentrations of oxygen experiment presented in Figures 30 and 31, little oxygen is needed to fully quench the luminescence of PtOEP. With such a high sensitivity, PtOEP-doped aerogels would not serve as a functional sensor for quantitative applications. However, the high sensitivity to oxygen would make PtOEP very capable as a switch, opening up a new array of applications.

III. Mixed PtOEP+R6G Aerogels

Figure 41 displays a time-based emission spectrum for a 10^{-6}-M PtOEP + R6G aerogel, with N_2 cycling.

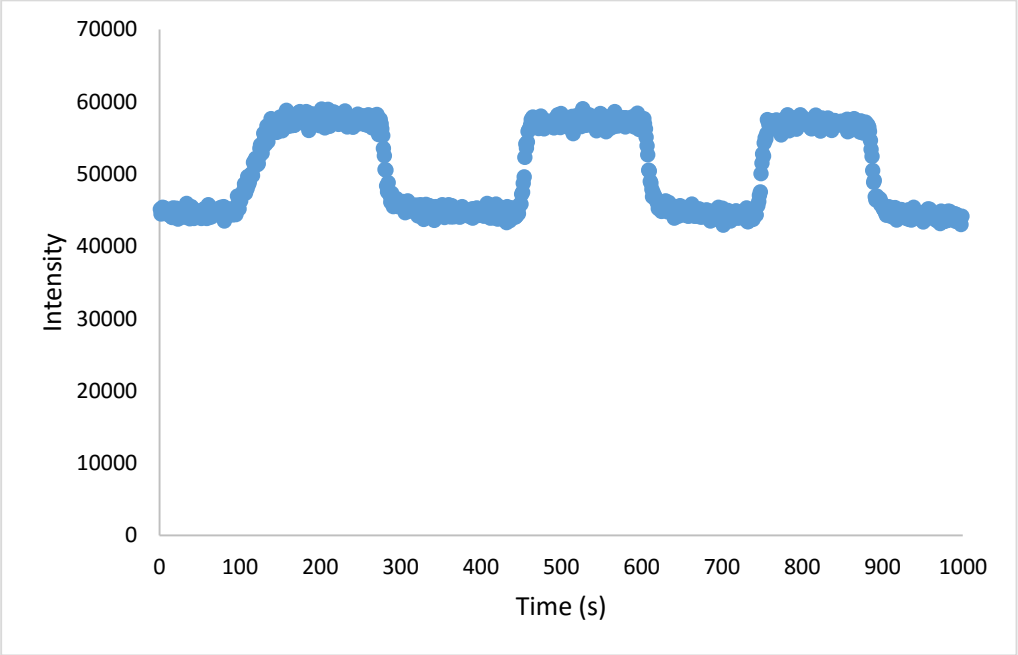

Figure 41: Time-based emission spectrum for 10^{-6}-M PtOEP + R6G monolith, sample B2 from batch Mix-A-1. The excitation wavelength was 533 nm, emission scan was at 643 nm, and there were 2 nm excitation and emission slit widths.

At 95, 450, and 740 s the N_2 tank was turned on purging the cuvette of O_2. At 275, 600 and 880 s the N_2 tank was turned off, allowing air to reenter the sample. The sample responded quickly to changes in O_2 concentration, and the intensity was reversible.

IV. Monolithic Testing Rig

Figure 42 is a photograph of the cracked, large $3x10^{-5}$-M PtOEP aerogel sample inside the proof-of-concept rig under ambient conditions. Figure 43 shows 532-nm light impinging on the monolith. Figure 44 is the same rig and sample in Figure 43, only with the excitation light filtered out through use of laser goggles. Luminescence of PtOEP is not observed under ambient conditions.

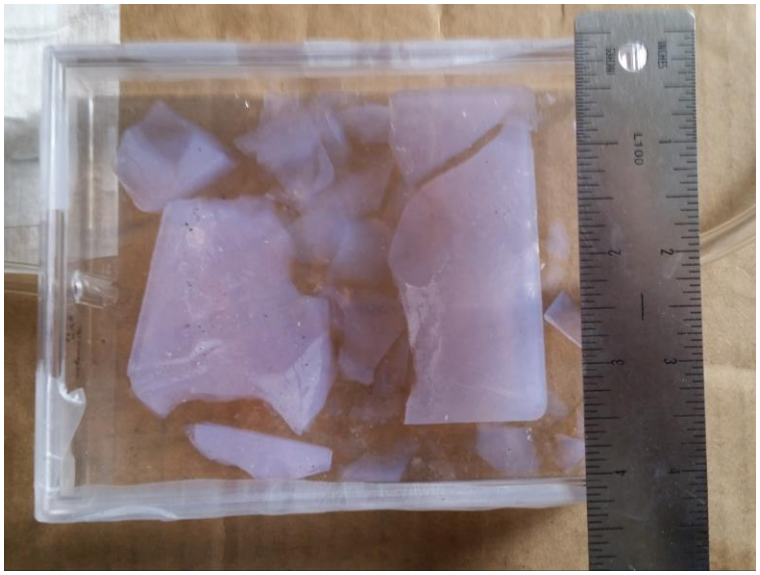

Figure 42: Proof-of-concept rig with large sample inside.

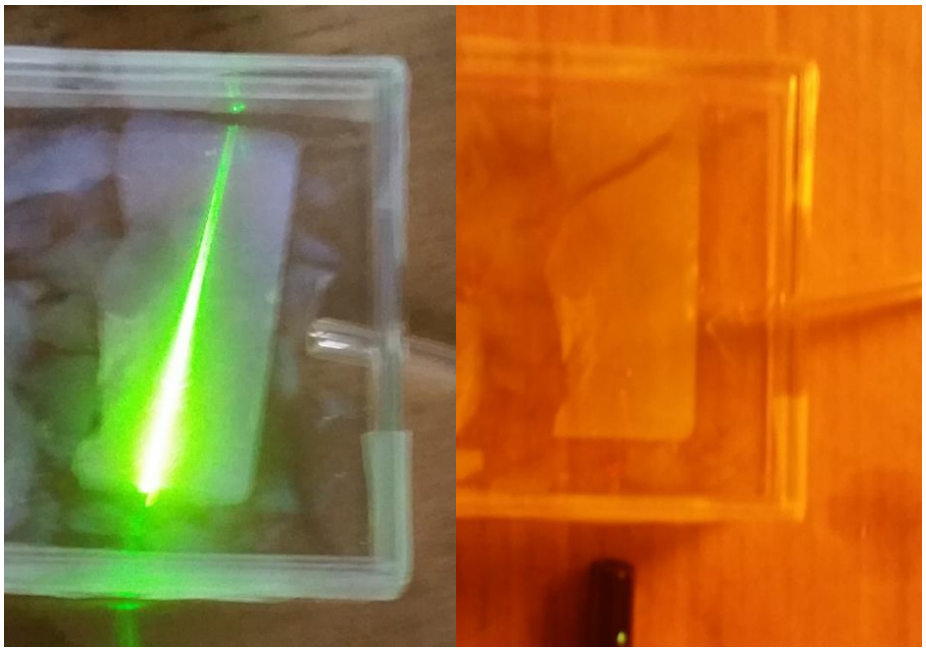

Figure 43: Left- Portion of large PtOEP monolith in translucent case with 532-nm laser pointer. Right- Portion of large PtOEP monolith under ambient conditions, imaged through laser goggles in the presence of O_2 with 532-nm laser excitation source.

Upon turning on N_2, the nitrogen flow displaces the ambient air, forcing the air through the outlet tubing, removing oxygen from inside the proof-of-concept rig. After removing the quencher, the luminescence is visible, as seen in Figure 44 as the bright red line.

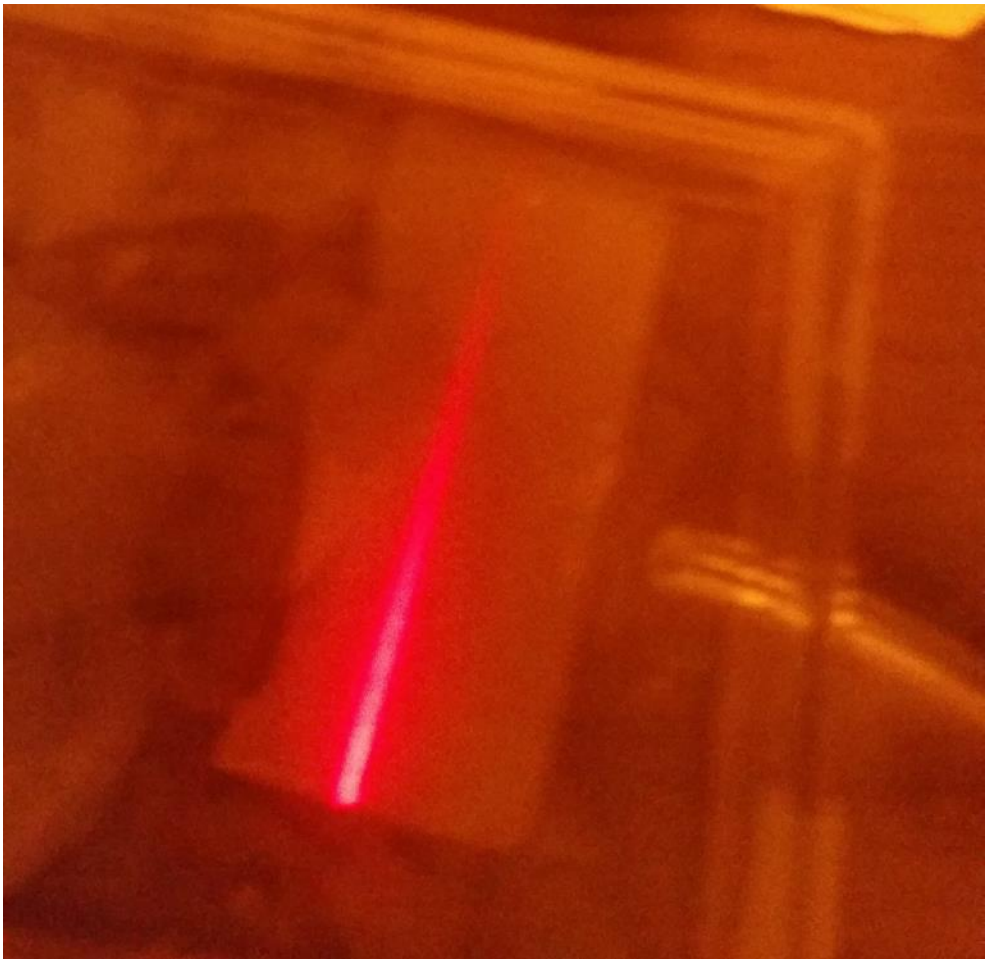

Figure 44: Luminescence emitted when sample was under constant N_2 flow (oxygen free environment).

Videos were taken through the laser goggles of the sample being excited with the laser pointer. The videos start out with the sample in the proof-of-concept rig under ambient conditions. No luminescence is noticeable due to the oxygen concentration in air. However, an N_2 tank is then turned on, allowing the nitrogen to flow into the rig. As nitrogen flowed into the rig, and displaced the oxygen, it was possible to see the luminescence where the laser pointer was directed. What was unique about this experiment is that the luminescence could be tracked as a function of time: the longer the N_2 was flowing into the rig, the more oxygen got displaced, and the luminescence appeared to "grow" from the edge of the sample closest to the laser

pointer, in a straight line along the excitation beam. Monitoring the direction of luminescence growth could be one way to determine the flow rate of gases through aerogels.

Conclusions and Future Work

All aerogel batches made using either of the 16-well molds produced two distinct types of aerogels. The samples from the outer wells were mostly the size of the wells, and exhibited densities consistent with silica aerogels. Samples from the four inner wells all shrunk significantly, usually to about a sixth of the size of the well. Density measurements indicate that these samples have some xerogel characteristics. It is likely a hot press issue, potentially uneven heat distribution or platens that are not completely parallel, that is causing all batches to have this inconsistency. The hot presses have been undergoing repairs the second half of this project, and it would be beneficial to see if there is still a discrepancy in the fabricated samples after they are fixed.

While Rhodamine 6G (R6G) wet gels had consistent emission spectra, once the samples start drying to xerogels the fluorescence peak would inconsistently blue shift. Not all R6G-doped aerogels fluoresced, as the outer-well 10^{-4}-M samples did not fluoresce. However, even the samples that did fluoresce did not change in response to concentration of oxygen in the area, agreeing with prior literature.[49] Rhodamine 6G would not be a beneficial oxygen sensor by itself, but moving forward could be used with an oxygen sensor such as PtOEP as a means to measure

[49] A. Kahn, et al. "Fabrication of Oxygen-Sensor Films for Detecting and Treating Infections." *Interfaces and Surfaces NSF REU Site* (2013)

the ratio of change of luminescence. Initial work has been done using combined R6G and PtOEP-doped aerogels, and that could be pursued further.

The effectiveness of our platinum (II) octaethylporphyrin (PtOEP)-doped aerogels is dependent on the probe surviving the hot press process. Based on our results, if the hot press reaches temperatures higher than 260 °C (500 °F), most of the PtOEP probes will thermally decompose.

Emission spectra for successfully fabricated PtOEP-doped aerogels taken under ambient conditions does not seem to indicate that they luminesce. At lower concentrations of oxygen, PtOEP-doped aerogels are shown to luminesce. However, as little as 0.06% O_2 in the environment decreases the luminescence by a factor of 4.1, from luminescence without a quencher present.

Time-based emission scans using N_2 indicate that PtOEP-doped aerogels are sensitive to oxygen, and exhibit a reversible response. Due to the high sensitivity of PtOEP-doped aerogels to oxygen, they might be better applied to applications requiring a switch than a sensor with wide dynamic range.

Since Stern-Volmer plots are not linear, it is apparent that not all the probes are located in the same microenvironment. Various modified plotting methods can be used. One model is the assumption that some of the probes are in accessible one site, and the rest in a separate, inaccessible site. When that assumption is employed, the best fits show that 90 and 97% of the probe is accessible to oxygen, for an outer-well and inner-well monolith, respectively. Another model is that of a two-site microenvironment system, applied to the Stern-Volmer plot using KaleidaGraph. For that assumption, the fits indicate that 92.5 and 98.2% of the probe is

accessible to oxygen in the main microenvironment, for an outer-well and inner-well monolith, respectively.

Experimentally, it has been determined that PtOEP-doped aerogels are scalable to 3.5 x 3.5 x 0.5”, and that the luminescence can be optically observed using the proper safety gear. While only one “larger” sample has been fabricated and observed in a proof-of-concept rig, much work should be put into quantifying this experiment in the future. The ability to see the luminescence “grow” through the sample as oxygen is displaced by nitrogen could serve to provide information into flow rates of gases through silica aerogels. Tracking the luminescence as a function of time could be used to monitor the rate of diffusion of oxygen and directionality of flow through the aerogel.

Acknowledgements

I would like to thank Prof. Mary Carroll, for her support and guidance these past two years in the aerogel lab. She has helped me develop into the researcher, and person, that I am today. I would also like to thank Prof. Ann Anderson and Prof. Bradford Bruno for their continued support throughout my time as a member of this lab group.

Thank you to Prof. Michael Hagerman for invoking in me a sense of awe about science and living as an example of an individual passionate about what they do. Professors Andrew Huisman, James McGarrah and Laura MacManus-Spencer have all lent instrumentation and equipment necessary to gathering the data that serves as the crux of this thesis. This material is based upon work supported by the National Science Foundation (NSF) under Grant. No DMR-1206631. If not for funds from the Union Student Conference Travel Grant and the Union College Chemistry Department, I would not have been able to present this information at the National ACS Conference in San Diego.

Many thanks to all the other members in the aerogel lab as we went on this journey together. Particularly, thank you to Elizabeth Donlon and Tyler Gurian, who provided the engineering knowledge to fill in my gaps, and to Stan Gorski and Paul Tompkins of the Union College Engineering Department for fabricating equipment necessary for this project.

Ultimately, none of this would have been possible without the years of support and inspiration from Dennis and Lucy Hawthorne. They taught me to pursue my interests and strive to be the best I could, regardless of the expectations of others. Lastly, thank you, curious science reader, for having taken the time to read through what I have spent many hours of rigorous intellectual prowess and dedication on. Stay class, world.